Title: Lynx1 modulates the activity of nAChRs to slow NMJ and muscle fiber degeneration during aging

Sydney K. Vaughan[1,2], Sebastian Barbat-Artigas[4], Tracey Myers[3], Bhola Pradham Shankar[5], Tomasz J. Prószyński[5], Richard Robitaille[4], Gregorio Valdez[1]

[1] Department of Molecular Biology, Cellular Biology, and Biochemistry, Brown University, Providence, Rhode Island, USA.

[2] Graduate Program in Translational Biology, Medicine, and Health, Virginia Tech, Blacksburg, Virginia, USA.

[3] Fralin Biomedical Research Institute, Roanoke, Virginia, USA.

[4] Département de neurosciences, Université de Montréal, Montréal, QC, Canada.

[5] Laboratory of Synaptogenesis, Nencki Institute of Experimental Biology, Polish Academy of Sciences, Warsaw, Poland.

Corresponding Author

Gregorio Valdez

Department of Molecular Biology, Cellular Biology, and Biochemistry

Brown University

70 Ship Street, Providence, RI, 02903

Email: Gregorio_Valdez@brown.edu

Keywords: development, plasticity, cholinergic transmission, aging, miniature endplate potential

Abstract

Cholinergic transmission must be tightly regulated at mammalian neuromuscular junctions (NMJs) for motor neurons and skeletal muscles to properly communicate and remain viable. Here, we examined the function of Lynx1, and endogenous regulator of cholinergic transmission, at NMJs in mice. We show that Lynx1 interacts with and modulates the activity of muscle nicotinic acetylcholine receptors (nAChRs) at NMJs. We also demonstrate that deletion of Lynx1 prematurely and progressively increases the incidence of NMJs with age-related features including fragmentation, nerve sprouting, and multiple innervation. Deleterious changes at NMJs lacking Lynx1 ultimately culminate in the atrophy and de-differentiation of muscle fibers from a fast to a slow phenotype, two hallmarks of aged skeletal muscles. Additionally, we show that Lynx1 is markedly reduced at aged NMJs of control mice, further indicating that Lynx1 plays important roles in mitigating age-related changes at NMJs. These data show that Lynx1 is an attractive target for preventing aging of NMJs and skeletal muscles.

Introduction

Neurotransmission is vital for proper communication across synapses in the central and peripheral nervous systems, and thus normal cognitive and motor functions[1]. In the somatic motor system, cholinergic transmission initiates all voluntary movements. This occurs at the synapse between motor neurons and skeletal muscles, called the neuromuscular junction (NMJ), where acetylcholine (ACh) released from motor axons binds to nicotinic acetylcholine receptors (nAChRs) on skeletal muscles and drives muscle contraction. Because of this critical role in voluntary movement, the cholinergic system is tightly regulated to ensure the proper development, function, and viability of skeletal muscles. For example, the composition and function of nAChRs pentamers changes during development, and in response to conditions that affect the availability of ACh[2]. As NMJs mature, the γ subunit of nAChRs is gradually replaced by the ε subunit[3–5]. The presence of the ε subunit reduces the open time of nAChRs, when bound to ACh, and therefore attenuates their activity. This transition, from nAChRs containing γ to ε subunits, is important for the normal development and function of adult NMJs, and thus skeletal muscles[6]. Highlighting this point, mutations in the ε subunit causes congenital myasthenic syndrome (CMS)[7–12], a neuromuscular disease characterized by muscle weakness and fatigue. The stability and function of adult nAChR pentamers has also been shown to depend on proper phosphorylation of its subunits and on associations with other key molecules involved in nAChR trafficking, clustering, and anchoring[13–18]. Thus, multiple mechanisms have been found to alter the properties of nAChRs to regulate the response of muscle fibers to changes in cholinergic transmission.

Evidence continues to accumulate indicating that changes in the cholinergic system may contribute to NMJ degeneration and muscle fiber atrophy[19–21]. In skeletal muscles of old animals and afflicted with amyotrophic lateral sclerosis (ALS), the γ subunit is elevated compared to muscles in healthy young adult mice[22,23]. There is also evidence indicating that presynaptic sites fail to adequately control the release of ACh in aged and ALS affected animals[24–26]. ACh acts as an anti-synaptogenic factor by directly promoting the disassembly of nAChR clusters[14], in addition to its classical role as a neurotransmitter. Through this action, a moderate yet consistent increased in the release of ACh from the random fusion of synaptic vesicles may destabilize nAChR clusters and thereby contribute to degeneration of NMJs during aging and in ALS. Supporting this possibility, we recently demonstrated that NMJs prematurely acquire age-associated features in transgenic mice which have increased levels of ACh in synaptic vesicles[27]. These published findings strongly suggest that aberrant cholinergic transmission may promote degeneration of adult NMJs and muscle fibers.

Although years of efforts have revealed the identity of many critical components of the cholinergic system at NMJs, it remains unknown if Lynx1 is present and modulates nAChRs at NMJs. Lynx1 is a GPI-anchored protein present on the cell surface shown to interact with and modulate the function of nAChRs in the central nervous system (CNS)[28–31]. In the brain, Lynx1 has been shown to modulate the activity of α7 and $\alpha_2\beta_4$ pentamers[30–32]. Lynx1 has also been found to inhibit neuronal plasticity in the visual and auditory cortex by reducing the sensitivity of nAChRs to ACh[33–35]. Additionally, there is evidence that while loss of Lynx1 augments motor learning during normal aging, it also contributes to neuronal degeneration in the dorsal striatum[36,37]. We therefore

hypothesized that Lynx1 is present and modulates the activity of muscle specific nAChR pentamers at NMJs.

We carried out complementary experiments to examine the function of Lynx1 in skeletal muscles, specifically at NMJs. We discovered that Lynx1 is indeed expressed in skeletal muscles and progressively concentrates at NMJs during development. Importantly, we show that Lynx1 interacts with and modulates the activity of nAChRs at the NMJ. We also found that while loss of Lynx1 does not affect developing NMJs, it accelerates the appearance of age-related features at NMJs in young adult and middle-aged mice. Furthermore, the deleterious changes at NMJs resulting from loss of Lynx1 ultimately cause muscle atrophy in adult mice. Consistent with these data from knockout mice, we found that Lynx1 is significantly decreased at aged NMJs of control mice. Together, these data show that Lynx1 modulation of nAChRs is important for the maintenance of NMJs and viability of muscle fibers.

Results

Muscles fibers express and concentrate Lynx1 in the postsynaptic region

We first sought to determine if Lynx1 is expressed in skeletal muscles, and specifically by muscle fibers. We examined Lynx1 transcripts in ribosomal mRNA fractions specifically isolated from fast-type muscle fibers within the tibialis anterior (TA) muscle. We accomplished this by crossing mice expressing the ribosomal protein Rpl22 tagged with HA epitopes[38] (RiboTag$^{flox/flox}$) with parvalbumin-Cre (PVCre) transgenic mice[39] to generate PVCre; RiboTag$^{flox/flox}$ offspring. HA-tagged Rpl22 is expressed in fast-type muscle fibers, which constitute the majority of muscle fibers in the TA muscle, in PVCre; RiboTag$^{flox/flox}$ mice. This approach revealed that Lynx1 transcripts are enriched

in ribosomal mRNA fractions obtained from the TA muscle compared with total muscle mRNA. (Fig. 1A). We then examined the temporal expression of Lynx1 in skeletal muscles of wild-type mice. We found that Lynx1 transcripts increase in the TA muscle as mice transition from postnatal to the juvenile stage of life (Fig. 1B). We validated these findings in C2C12-derived myotubes, which increase expression of Lynx1 as they mature (Fig. 1C). Importantly, we immunostained skeletal muscles for Lynx1 and found Lynx1 localized at the NMJ, based on staining of nAChRs using fluorescently tagged α-bungarotoxin (BTX) (Figure 1D-E). This analysis also showed that Lynx1 protein gradually increases and specifically at NMJs during development (Fig. 1F). Thus, muscle fibers express and concentrate Lynx1 in the postsynaptic region of the NMJ.

Lynx1 interacts with nAChRs of the NMJ

The findings above, along with published data[28,30–32,40,41], suggest that Lynx1 accumulates in the postsynaptic region of the NMJ to interact with and modulate the activity of nAChRs. To test the first possibility, we performed a series of biochemical experiments. To start, we used homogenates from HEK293 cells co-transfected with mCherry-tagged Lynx1 and four different muscle nAChR subunits (alpha, beta, delta, and epsilon). Because these four subunits assemble at the peripheral membrane, this co-transfection strategy allowed us to test the interaction between Lynx1 and nAChR pentamers. Following immunoprecipitation with a pan-antibody against the nAChR pentamer and western blotting, we found that Lynx1, revealed using an antibody against mCherry, is only pulled down from cells co-transfected with the nAChR subunits (Fig. 2A). We then asked if Lynx1 interacts with a specific subunit of the nAChR pentamer. For this, we generated recombinant alpha, beta, delta, epsilon, and gamma nAChR subunits

tagged with glutathione S-transferase (GST). We used these recombinant proteins to coat GST beads to precipitate mCherry-Lynx1 from HEK293 lysates. As shown in figure 2B, all nAChR subunits precipitated Lynx1 fusion protein, indicating that Lynx1 may bind to each nAChR subunit. Finally, and most importantly, we asked if the interaction between nAChRs and Lynx1 is direct or indirect. We performed classical pull-down experiments after incubating purified GST-Lynx1 with the ectodomain of the alpha subunit also tagged with GST. In this case, the GST-tagged alpha subunit was pulled-down with bungarotoxin coated beads. We again found that Lynx1 co-precipitates with the alpha subunit revealed by Western blot with anti-GST antibody (Fig. 2C). To validate this finding, we purified and incubated 6-His-Lynx1 with the extracellular portions of each nAChR subunit, alpha, beta, delta, epsilon, and gamma, tagged with GST. We then immunoprecipitated the nAChR subunits using anti-GST coated beads. As shown in figure 2D, each nAChR subunit co-precipitated 6-His-Lynx. Collectively, these experiments strongly indicate that Lynx1 directly interacts with all the nAChR subunits.

Lynx1 modulates the sensitivity of nAChR to ACh in skeletal muscles

The association between Lynx1 and nAChRs in skeletal muscles suggests that Lynx1 functions to regulate cholinergic activity at the NMJ. To determine the function of Lynx1 at the NMJ, we first examined miniature endplate potentials (MEPPs), as they directly reflect properties of postsynaptic receptors. Using NMJs from 4-month-old Lynx1$^{-/-}$ mice and controls (Fig. 3A-B), we observed that the mean amplitude and frequency of MEPPs are unchanged in NMJs lacking Lynx1 (Fig. 3C-D). However, the rise time, which reflects the binding of ACh to its receptors, was significantly faster in Lynx1$^{-/-}$ NMJs compared to controls (Control=1.33±0.0952ms; Lynx1$^{-/-}$=0.857±0.1321ms, p=1.66E-27;

Fig. 3E). Supporting this finding, the slope to reach the maximum MEPP amplitude is steeper at NMJs lacking Lynx1 (Fig. 3F). However, loss of Lynx1 does not alter the EPP amplitude (Fig. 4A-B), or the quantal content (Fig. 4C) at NMJs. These data indicate that while the binding of nAChRs to ACh and the postsynaptic response was facilitated, the probability of ACh release remains unaltered at NMJs in Lynx1$^{-/-}$ mice.

We next asked if synaptic plasticity events elicited by sustained motor nerve stimulation (120 Hz, 10 s) were altered in NMJs lacking Lynx1. At NMJs of control mice, we observed a rapid and short-lasting depression (74.96±1.589%; Fig. 4D) that was followed by a delayed, long-lasting depression (11.88±3.635%; Fig. 4D). However, in NMJs of Lynx1$^{-/-}$ mice, while the rapid and short-lasting synaptic depression was unchanged (77.74±1.553%; Fig. 4D), we observed a significant post-tetanic potentiation (12.22±3.688%) and the delayed, long-lasting depression, was obliterated (Fig. 4D).

We also tested the possibility that altered synaptic properties in Lynx1$^{-/-}$ NMJs may lead to changes in muscle function. We used a force transducer to measure the contractile properties of the EDL muscle following either direct muscle stimulations or nerve-evoked synaptic activity to elicit contractions. We found that muscles lacking Lynx1 generated less force when stimulated directly (Control=59.16±2.243%; Lynx1$^{-/-}$=47.15±3.831%, p=0.0186 at 1min; Fig. 4E), whereas responses remained the same when nerve-evoked. This data shows that loss of Lynx1 compromises the function of skeletal muscles.

Lynx1 is not required at NMJs and muscle fibers during development

We found that Lynx1 expression and localization at NMJs progressively increases as muscle fibers mature (Fig. 1). These findings suggested that Lynx1 may play roles in the maturation and stability of NMJs and muscle fibers. To start looking into this

possibility, we examined the impact of deleting Lynx1 on developing NMJs and muscle fibers in the EDL and soleus muscles of postnatal day 6 (P6) mice. This is an age when NMJs and muscle fibers are undergoing fast and dramatic morphological, molecular, and functional changes in mice[42]. This analysis showed no significant morphological differences in NMJs and muscle fibers between control and Lynx1$^{-/-}$ mice (Supplementary Figure 1A-J). Furthermore, there were no differences in levels of the α, β, δ, ε, or γ nAChR subunits in Lynx1$^{-/-}$ mice compared to control mice (Supplementary Figure 1K). Similarly, the expression of acetylcholinesterase (AChE), Muscle-Specific Kinase (MuSK), Low-density lipoprotein receptor-related protein 4 (LRP4), and Receptor-Associated Protein of the Synapse (Rapsyn) remained unchanged in Lynx1$^{-/-}$ mice compared to control mice at P6 (Supplementary Figure 1L-O). Together, these findings show that Lynx1 is not required for the proper cellular and molecular maturation of the NMJ.

To determine if the loss of Lynx1 affects the maturation of muscle fibers, we analyzed TA muscles from P6 Lynx1$^{-/-}$ and control mice. As expected, based on our analysis of NMJs, there were no significant differences in the average muscle fiber area or frequency distribution of muscle fiber areas in Lynx1$^{-/-}$ mice compared to controls (Supplementary Figure 2A-D). The incidence of muscle fibers with centralized nuclei, a proxy for immature and also regenerating muscle fibers, is unchanged at P6 in mice lacking Lynx1 compared to age-matched control mice (Supplementary Figure 2E). Molecularly, there were no significant differences in the expression profile of myosin heavy chains I, IIa, IIb, and IIx in Lynx1$^{-/-}$ mice compared to control mice (Supplementary Figure 2F). The loss of Lynx1 also did not impact the expression of two pro-myogenic

196 genes, Pax7[43] or myogenin[44] (Supplementary Figure 2G-H). Taken together, these data
197 show that Lynx1 is not required for the proper and timely maturation of muscle fibers.

198 ***Lynx1 functions to stabilize the NMJ***

199 Lynx1 concentration is highest at adult NMJ (Fig. 1) where it modulates the activity
200 of nAChRs (Fig. 3, Fig. 4). To further discern the role of Lynx1 in skeletal muscles, we
201 then examined the impact of deleting Lynx1 on adult NMJs in the EDL muscles of 4-
202 month-old mice. This analysis revealed several structural differences at NMJs of Lynx1$^{-/-}$
203 compared to control mice (Fig. 5A-B). These included a significant increase in the number
204 of denervated and fragmented NMJs in Lynx1$^{-/-}$ compared to control mice (Fig. 5C). Even
205 though the size of the NMJ was unchanged (Fig. 5D), there was a marked reduction in
206 the density of nAChRs in the postsynaptic region in Lynx1$^{-/-}$ compared to control mice
207 (Fig. 5E). Additionally, adult Lynx1$^{-/-}$ mice had more motor axons with large blebs proximal
208 to the NMJ (Fig. 5F). Despite these changes, muscle fibers remained largely singly
209 innervated in in Lynx1$^{-/-}$ compared to control mice (Fig. 5F). Because of these findings,
210 we were not surprised to find transcripts for each nAChR subunit, MuSK, and LRP4
211 significantly elevated in skeletal muscles lacking Lynx1 (Fig. 5G-I). However, Rapsyn was
212 decreased in Lynx1$^{-/-}$ mice (Fig. 5J). These data support immunohistochemical analysis
213 showing reduced intensity of nAChRs at NMJs lacking Lynx1 (Fig. 5E) for two reasons.
214 First, it has been shown that nAChR subunits, MuSK and LRP4 are increased to
215 compensate for loss of nAChR pentamers[45]. Second, the decreased expression of
216 Rapsyn, which anchors nAChR clusters to the plasma membrane in a 1:1 stoichiometry[46],
217 demonstrates that nAChR pentamers are unstable and likely turnover at a faster rate in
218 muscles lacking Lynx1. Additionally, we found acetylcholinesterase (AChE) increased in

Lynx1$^{-/-}$ mice (Fig. 5K). As shown below, we hypothesize that muscle fibers lacking Lynx1 increase levels of AChE because of augmented sensitivity of nAChRs to ACh, and not as a result of higher levels of ACh at the synaptic cleft. Altogether, these findings demonstrate that Lynx1 plays important roles at adult NMJs.

Based on the above findings, we hypothesized that NMJs lacking Lynx1 would continue to accrue age-related features at a faster rate with advancing age. To test this hypothesis, we extended our analysis to middle-aged, 12-month-old, mice (Fig. 6A-B). We again found a higher incidence of denervated and fragmented NMJs in middle-aged Lynx1$^{-/-}$ mice compared to age- and sex-matched control mice (Fig. 6C). Middle-aged Lynx1$^{-/-}$ mice also presented with smaller receptor area (Fig. 6D) and reduced nAChRs density, revealed by the lower intensity of BTX (Fig. 6E). Additionally, middle-aged Lynx1$^{-/-}$ mice had more multiply innervated NMJs and innervating motor axons with large blebs, a hallmark of degenerating axons (Fig. 6F). This data showed that NMJs lacking Lynx1 accrue additional age-related features. To complement this cellular data, we again examine expression of genes critical for the stability and function of the NMJ. We found most nAChR subunits expressed at lower levels in middle-aged Lynx1$^{-/-}$ mice compared to age-matched control mice (Fig. 6G). Interestingly, these expression patterns of nAChR subunits are in contrast to those of young adult mice (Figure 5G). MuSK, LRP4, and Rapsyn were unchanged in middle-aged Lynx1$^{-/-}$ mice compared to age-matched control mice (Fig. 6H-J). AChE was found decreased in middle-aged Lynx1$^{-/-}$ mice compared to age-matched control mice (Fig. 6K). These findings suggest that skeletal muscles lacking Lynx1 prematurely lose the capacity to recruit compensatory mechanisms important for stabilizing and repairing damages at NMJs with advancing age.

Increased nAChR turnover in Lynx1 null mice

In mice lacking Lynx1, there is a marked reduction in the density of nAChRs at NMJs. Since Lynx1 binds to these receptors, it raised the possibility that Lynx1 also functions to stabilize nAChRs at the membrane. To test this possibility, we examined the rate of nAChRs turnover in the sternomastoid muscle of 3-month-old Lynx1$^{-/-}$ and control mice following in vivo labeling with saturating levels of alexa-488 conjugated BTX (A488-BTX). We then used alexa-555 conjugated BTX (A555-BTX) to reveal newly inserted nAChRs at NMJs[47] (Fig. 7A-C). Demonstrating the validity of this approach, A555-BTX failed to label NMJs in the sternomastoid when it was fixed immediately following exposure to saturating concentrations of A488-BTX (Supplementary Figure 3). We analyzed the intensity profile of alexa-488 and alexa-555 labeled nAChRs to determine the ratio of new to old nAChRs across the endplate region (Fig. 7D-E). In the sternomastoid of Lynx1$^{-/-}$ mice, the average ratio of new to old nAChRs at NMJs was significantly higher compared to control mice (Fig. 7F). During the course of this experiment, we observed considerable variability in A555-BTX staining among NMJs within sternomastoid muscles from the same animal. We attributed this variability to differences in nAChR turnover rates due to varied functional demands on NMJs within the same muscle. To account for this variability across NMJs, we examined the frequency of NMJs with specific ratios of new to old nAChRs. We again found significantly more NMJs with a higher ratio of A555-BTX to A488-BTX, and thus newer nAChRs, in Lynx1$^{-/-}$ mice (Fig. 7G). These data show that Lynx1 functions to stabilize nAChRs at NMJs in addition to modulating their sensitivity to ACh.

Muscle atrophy follows deleterious changes at NMJs in mice lacking Lynx1

Even though Lynx1 concentrates and modulates the function of nAChRs at NMJs, it is plausible that NMJs lacking Lynx1 accrue deleterious features resulting from changes elsewhere in muscle fibers or motor neurons. To address this possibility, we first examined muscle fibers for signs of atrophy and turnover in 4- and 12-month-old mice with and without Lynx1. To compare changes in muscle size between genotypes and thus determine if deletion of Lynx1 causes atrophy, we measured the cross-sectional area (CSA) of individual muscle fibers and the whole TA muscle. We used the same samples to determine the location of myonuclei, with those located away from the peripheral membrane indicating that the muscle fiber had degenerated and regenerated. This analysis revealed no difference in the average muscle fiber CSA (Supplementary Figure 4A-C) and in the CSA frequency distribution of individual muscle fibers between 4-month-old Lynx1$^{-/-}$ and control mice (Supplementary Figure 4D). The CSA of the whole TA muscle was also unchanged in 4-month-old Lynx1$^{-/-}$ compared to control (Supplementary Figure 4E). Similarly, the occurrence of centralized myonuclei was unchanged in young adult Lynx1$^{-/-}$ (Supplementary Figure 4F). Hence, we found no obvious signs of muscle fiber atrophy in mice lacking Lynx1 at 4 months of age even though NMJs have clearly begun to degenerate at this age (Fig. 5).

We also examined the expression of genes associated with the formation, health and identity of muscle fibers. There was a significant reduction of Pax7 and myogenin levels in Lynx1$^{-/-}$ compared to control mice (Supplementary Figure 4G, H), two genes important for myogenesis. Additionally, we found a marked increase in levels of atrogin-1 and Forkhead Box O1 (FOXO-1), which promote muscle atrophy, in 4-month-old Lynx1^{-}

$^{/-}$ mice compared to age-matched control mice (Supplementary Figure 4I, J). As previously shown[19,21], these molecular alterations may be driven by dysregulated cholinergic transmission at NMJs resulting from loss of Lynx1. However, the loss of Lynx1 had no effect on levels of myosin heavy chains I, IIa, IIb, and IIx in the TA muscle at 4 months of age (Supplementary Figure 4K).

Since NMJs continue to degenerate with advancing age in mice lacking Lynx1, we surmised that muscle fibers would ultimately atrophy and exhibit signs of regeneration in older mice. Indeed, the average muscle fiber CSA was significantly reduced in 12-month-old Lynx1$^{-/-}$ mice compared to age- and sex-matched control mice (Fig. 8A-C). In the TA muscle of Lynx1$^{-/-}$ mice, the overall size reduction resulted from the presence of more muscle fibers with a reduced CSA, revealed using a cumulative frequency histogram plot (Fig. 8D). Not surprisingly, the CSA of the whole TA muscle was significantly smaller in 12-month-old Lynx1$^{-/-}$ compared to control (Fig. 8E). Supporting these findings, muscle fibers lacking Lynx1 were populated with more centralized myonuclei (Fig. 8F). Additionally, we found that Pax7 was significantly reduced in the TA muscle of middle-aged Lynx1$^{-/-}$ mice compared to controls of the same age (Fig. 8G). However, myogenin was increased (Fig. 8H) while atrogin-1 was unchanged, and FOXO-1 was reduced in 12-month-old Lynx1$^{-/-}$ mice compared to control mice (Fig. 8I, J).

In addition to muscle atrophy, aging causes fast-type muscle fibers to de-differentiate into slow types[48–50]. To determine if this shift occurs prematurely in mice lacking Lynx1, we visualized muscle fiber types using antibodies against MYHCIIa and MYHCIIb (Fig. 9A-C). We found fewer MYHCIIb-positive muscle fibers and more muscle fibers that were either MYHCI or MYHCIIx in Lynx1$^{-/-}$ mice (Fig. 9D). To corroborate these

findings, we assessed transcript levels for each myosin heavy chain and found a significant increase in MYHCI expression in Lynx1$^{-/-}$ muscles compared to age-matched controls (Fig. 9E). These data show that loss of Lynx1 affects the identity, and importantly the viability of muscle fibers. However, these myogenic changes occur after NMJs lacking Lynx1 have accrued significant functional and structural deleterious features (Fig. 5).

Motor neurons do not atrophy in Lynx1$^{-/-}$ mice

Lynx1 was found to be expressed in the ventral horn of the spinal cord[51], where motor neurons reside. This raised the possibility that global deletion of Lynx1 may also compromise the function and health of motor neurons. In this case, the changes observed at NMJs of mice lacking Lynx1 may result from alterations in motor neurons. However, we found no difference in the size of motor neurons between Lynx1$^{-/-}$ and control mice at 4 and at 12 months of age (Supplementary Figure 5). This finding along with electrophysiological recordings indicating normal EPP, a readout of presynaptic function, indicate that global deletion of Lynx1 does not alter the viability and function of motor neurons. Moreover, these data further indicate that deletion of Lynx1 causes pathological changes first at NMJs, which then compromises the viability of skeletal muscles.

Lynx1 is reduced at aged NMJs

Finally, we asked if aberrant changes in Lynx1 may contribute to the inevitable degeneration of NMJs that occurs with advancing age in control mice. We compared Lynx1 distribution and expression between old and young NMJs. Immunostaining and light microscopy analysis showed that Lynx1 is markedly reduced in NMJs of 24-month-old compared to 4-month-old mice (Fig. 10A-C). The loss of Lynx1 from aged NMJs does not result from decreased expression since its transcripts were found expressed at similar

levels in the TA muscle of old and young mice (Fig. 10D). The decreased concentration of Lynx1 at aged NMJs was also uncorrelated with changes in expression of most nAChR subunits, as most were increased in aged compared to young skeletal muscles (Fig. 10E). This finding mirrors the expression pattern of nAChRs in 4-month-old mice lacking Lynx1. Thus, the loss of endogenous Lynx1 from aging NMJs may contribute to the instability of nAChRs and thereby age-related neuromuscular degeneration.

Discussion

Lynx1, an endogenous regulator of cholinergic activity, was first described in 1999 in the brain[28]. Initial reports revealed structural similarities between Lynx1 and α-bungarotoxin, which binds with high affinity to nAChRs. The GPI anchor, which attaches Lynx1 to the membrane[28], primarily distinguishes Lynx1 from α-bungarotoxin and other neurotoxins. Further analysis confirmed that Lynx1 interacts with nAChRs and functions to maintain a low sensitivity to ACh, contributing to the synaptic safety margin[31]. In addition to interacting with nAChRs on the peripheral membrane, Lynx1 binds to nAChRs in the endoplasmic reticulum where it shifts the stoichiometry of subunits to generate a nAChR pentamer with lower sensitivity to ACh[32]. This interaction within the endoplasmic reticulum has been suggested to be mediated through the preferential binding of Lynx1 to specific subunit interfaces[30]. Analysis of Lynx1 knockout mice has provided valuable insights into its role in vivo. Lynx1 was found to be an allosteric modulator of nAChRs, critical for neuronal survival[40]. More recently, Lynx1 has been implicated in neuronal plasticity[34,35,52], motor learning[37], aging[36], Alzheimer's[53], nociception[54], and nicotine addiction[29].

Despite the essential role nAChRs play at NMJs, Lynx1 had yet to be studied in skeletal muscles, and specifically at NMJs. As Dr. Zach Hall eloquently wrote in 1999, "A physiological role for Lynx1 at [the neuromuscular junction] would bring the α neurotoxin story full circle in a historically fitting and entirely satisfying way"[55]. Previous studies using a water-soluble version of Lynx1, which lacks the GPI anchor, found competitive binding between Lynx1 and α-bungarotoxin in AChBP and *T. californica* nAChRs and identified residues responsible for this interaction[41,56]. These data indicated for the first time that Lynx1 could potentially interact with muscle nAChRs. However, many questions remained regarding Lynx1 at NMJs. This included whether Lynx1 interacts with and modulates the activity of mammalian nAChRs and the biological significance of this function on the maintenance and stability of NMJs.

This study examined the role of Lynx1 in skeletal muscles, and particularly at NMJs in mice. We show that Lynx1 expression increases and concentrates at NMJs during development. We also demonstrate that Lynx1 vacates NMJs with advancing age. Importantly, we provide data revealing the function of Lynx1 at the NMJ. We demonstrate that Lynx1 interacts with nAChRs to impact synaptic and muscle properties. It also functions to stabilize nAChRs at the NMJ. Additionally, we show that Lynx1 plays a critical role in slowing the appearance of age-related pathological features in NMJs that culminate in the atrophy of muscle fibers. Thus, this study demonstrates that Lynx1 modulates the activity of nAChRs to preserve the function and structure of NMJs and muscle fibers.

We found that Lynx1 progressively increases when significant morphological and functional changes are occurring at maturing NMJs and muscles fibers[42]. However,

deletion of Lynx1 did not cause obvious morphological and molecular changes in developing NMJs and muscle fibers. Why then do developing muscle fibers progressively increase the expression of and concentrate Lynx1 at the NMJ? We hypothesize that Lynx1 upregulation may be a preparatory step to ensure that the cholinergic system functions optimally in matured and less plastic NMJs and skeletal muscles. We base this hypothesis on the fact that adult, but not developing, NMJs are susceptible to a rather moderate increase in cholinergic transmission[19]. It is also worth noting that in immature muscles, the presence of the γ subunit potentially negates the further sensitization of nAChRs to ACh caused by loss of Lynx1.

The data in this study, however, do support important roles for Lynx1 in maintaining the normal function and stability of adult NMJs by modulating the activity of nAChRs. They are also in line with published findings indicating that aberrant changes in the cholinergic system contribute to aging of the NMJs and skeletal muscles. For example, numerous studies have shown increases in the amplitude and/or frequency of miniature endplate potentials (MEPPs), which represent the random fusion of vesicles at active zones, endplate potentials (EPPs), and spontaneous giant miniature endplate potentials (GMEPPs), which occur when ACh is released from vesicles residing outside the active zone, in various skeletal muscles in old age[26,57–59]. These findings were confirmed in a recent study that compared cholinergic transmission at NMJs of 12-14 month-old versus 24-28 month-old mice[60]. Demonstrating that augmented cholinergic transmission contributes to NMJ degeneration, our lab recently showed that a moderate increase in MEPP amplitude resulting from elevated ACh causes NMJs to prematurely acquire age-related morphological features in young adult mice[27]. Thus, the loss of Lynx1 from aged

NMJs likely augments the activity of nAChRs, further exacerbating the deleterious effects of dysregulated cholinergic transmission that occurs with advancing age. Given that Lynx1 stabilizes nAChRs at the postsynapse, its loss may also underlie the instability of nAChRs at aged NMJs[17,61–63].

While this study unraveled a number of key roles of Lynx1 at NMJs and in skeletal muscles, it also raised a number of additional questions. This includes the identity of molecular mechanisms, influenced by cholinergic activity, that regulates the expression of Lynx1. This study also did not address the underlying reason for the loss of Lynx1 from aged NMJs. Additionally, it remains unknown if the absence of Lynx1 accelerates the turnover of nAChRs at NMJs by causing physical instability, or by changing their phosphorylation status due to increased binding to ACh. Answers to these questions would serve as the basis to preserve and restore the function of Lynx1 along with proper cholinergic transmission. Because of its role in modulating cholinergic transmission, Lynx1 is a promising candidate for mitigating the ravages of aging and other conditions, including ALS, nerve injuries and myasthenia gravis, all of which are known to alter cholinergic transmission and have either negative or positive actions on NMJs and muscles fibers[64–66]. Lynx1 may also confer benefits to muscle recovery following exercise where again cholinergic transmission fluctuates[67]. Thus, future studies should determine the specific role for Lynx1 in different conditions and at specific stages when cholinergic transmission is either heightened or diminished.

Methods

Source of mice

We obtained Lynx1$^{-/-}$ mice[40] from the lab of Dr. Morishita and began a colony of our own. These mice were mated with Thy1-YFP16[68] (RRID:IMSR_JAX:003709) animals in our colony to generate Lynx1$^{-/-}$;Thy1-YFP animals. In order to have littermate pairs, Lynx1$^{+/-}$;Thy1-YFP mice were mated together to yield litters with Lynx1$^{-/-}$;Thy1-YFP and Thy1-YFP control mice. The colony is maintained on a C57BL/6 background. The following mice were obtained from The Jackson Laboratory: Parvalbumin-Cre[39] (RRID:IMSR_JAX:017320), and RiboTag[38] (RRID:IMSR_JAX:011029) and bred to generate PVCre; RiboTag$^{flox/flox}$ offspring. Mice were anesthetized with isoflurane, followed by immediate dissection and collection of fresh tissues, or by transcardial perfusion with 1XPBS (pH 7.4) followed by 4% paraformaldehyde (PFA, pH 7.4) for fixed tissues. All experiments were carried out under the NIH guidelines and animal protocols approved by the Virginia Tech Institutional Animal Care and Use Committee or in accordance with the guidelines of the Canadian Council of Animal Care and the Comité de déontologie animale of Université de Montréal.

C2C12 cultures

C2C12 cells were plated in 8-well Flexiperm chambers on perminox slides coated with Poly-L-Ornithine (3 µg/mL; Sigma-Aldrich; P2533) and laminin in Dulbecco's Modified Eagle Medium (DMEM; 10 µg/mL; Thermo Fisher Scientific; 23017015). The myoblasts were plated at 100,000 cells per well in culture media (high-glucose DMEM, 20% fetal bovine serum, 1× Glutamine, pen-strep, Fungizone) and incubated at 37°C and 5.0% CO_2. Twenty-four hours post-plating, the media was replaced with fusion media (high-

glucose DMEM, 10% horse serum, 1× Glutamine, Pen strep, Fungizone). Myoblasts were then incubated for 3 to 7 days following the addition of fusion media to generate myotubes. RNA was extracted from myotubes before fusion, 3, and 7 days post-fusion using an Aurum Total RNA mini kit (Bio-Rad), following manufacturer's instructions.

Co-immunoprecipitation

Plasmid Constructs: For the GST pull-down experiments and co-immunoprecipitation studies, the coding sequences of extracellular domain of AChR subunits (α [amino acids 21-230], β [aa 26-238], δ [aa 25-248], ε [aa 21-239], and γ [aa 23-240], the signal sequences were removed) were cloned into pGEX-4T1 vector. The coding sequence of Lynx1 (amino acids 21-92) with the signal sequence and the GPI anchoring signal removed (Reference: PMID: 21252236) was cloned either into pGEX-4T1 vector (for GST tag) or pET-28a (+) vector for 6-His tag. The set of plasmids encoding the full-length α, β, δ, and ε subunits of AChRs was a kind gift from Dr. Lin Mei (Augusta University, USA). The plasmid pLynx1-mCherry, as described in Nichols et al.[18], was obtained from Dr. Henry A. Lester through Addgene.

Protein purification: Bacteria expressing the GST-tagged proteins were incubated in the GST lysis buffer (50 mM NaH2PO4, 300 mM NaCl, 10 µg/ml leupeptin, 10 µg/ml aprotinin, 1 µl/ml Triton X-100, 10 µg/ml DNase I, and 15 units/µl Lysozyme). Similarly, bacteria expressing the 6-His tagged proteins were incubated in the His lysis buffer (50 mM Tris-Cl (pH8.0), 100 mM NaCl, 5 mM Imidazole, 10 µg/ml leupeptin, 10 µg/ml aprotinin, 1 µl/ml Triton X-100, 10 µg/ml DNase I, and 15 units/µl Lysozyme). The supernatants containing the GST-fusion or 6-His fusion proteins were incubated overnight with 20 µl of equilibrated glutathione beads and His60 Ni resin, respectively. The beads containing GST-tagged

proteins were washed three times with the GST -wash buffer (4.3 mM Na2HPO4, 1.47 mM KH2PO4, 137 mM NaCl, and 2.7 mM KCl). Similarly, the beads containing 6-His-tagged proteins were washed three times with His wash buffer (50 mM Tris-Cl (pH8.0), 100 mM NaCl, 20 mM Imidazole). The proteins were eluted with elution buffer (10 mM glutathione 50 mM Tris pH=8,0 for GST tagged protein and 200 mM imidazole in 50 mM NaCl, 50 mM Tris pH=8,0 for 6-His tagged protein).

Immunoprecipitation: HEK293 cells were co-transfected with pLynx1-mCherry and four subunits of AChR (α, β, δ and ε); the cells were lysed 36 hr after transfection, and the immunoprecipitation was performed as previously described[69]. Briefly, the lysates were centrifuged, and supernatants were incubated with Dynabeads (Cat No: 10003D; Invitrogen, CA) and coated with anti-AChR antibody (Cat No: 838301, Biolegend, CA). Beads were then washed three times with lysis buffer, resuspended in 2x sample buffer and boiled for 5 min. The samples were resolved by SDS-PAGE electrophoresis and analyzed with anti-RFP antibody (Cat No: 600-401-379, Rockland, PA).

Purification of nAChR extracellular domains and Lynx1: The GST-tagged ectodomains of AChR subunits and Lynx1 (GST tagged or 6-His tagged) were purified as previously described[70]. BL21 bacteria were transformed with the respective constructs, grown in 200 ml cultures at 18°C until A600 between 0.4 and 0.6. The expression was induced by 0.5 mM isopropyl 1-thio-β-d-galactopyranoside (IPTG) for 4 h at 18 °C. Bacteria were collected, incubated for 30 min at 4 °C in lyses buffer (50 mM NaH2PO4, 300 mM NaCl, 10 µg/ml leupeptin, 10 µg/ml aprotinin, 1 µl/ml Triton X-100, 10 µg/ml DNase I, and 15 units/µl Lysozyme), lysed by sonication for 1 min, and centrifuged at 13,8 g for 30 min. The supernatants containing the GST-fusion proteins were incubated overnight with 20

µl of equilibrated glutathione beads. The beads were washed three times with washing buffer (4.3 mM Na2HPO4, 1.47 mM KH2PO4, 137 mM NaCl, and 2.7 mM KCl) and the proteins were eluted with elution buffer (10 mM glutathione 50 mM Tris pH=8,0). Purified GST-tagged proteins were used to coat 10 µl of glutathione beads. These were washed three times with washing buffer, followed by addition of homogenates of HEK293 cells transfected with pLynx1-Cherry, and then overnight incubation. The beads were washed with washing buffer and boiled with 2x sample buffer. The precipitated proteins were resolved by SDS-PAGE electrophoresis and detected with anti-Cherry or anti-GST (Cat No: G7781, Sigma, St. Louis, MO) antibodies.

To determine the direct interaction of GST-Lynx1 with the ectodomain of α subunit of AChR (GST-tagged), the GST-AChR protein was incubated with Streptavidin – Dynabead (Cat No: 11205D, Thermo Fisher Scientific, MA) coated with BTX-biotin (Cat No: B1196, Thermo Fisher Scientific, MA) for one hour. Beads were then washed three times with lysis buffer, and incubated with the purified GST-Lynx1 overnight. Beads were then washed three times with lysis buffer, resuspended in 2x sample buffer and boiled for 5 min. The samples were resolved by SDS-PAGE electrophoresis and analyzed with anti-GST antibody.

For analyzing Lynx1 specificity for AChR subunits, purified GST-tagged AChR subunits were used to coat 20 µl of glutathione beads. These beads were washed three times with washing buffer, followed by incubation with the purified 6-His-Lynx1 overnight. The beads were washed with washing buffer and eluted with elution buffer (10 mM glutathione 50 mM Tris pH=8,0). The eluted proteins were mixed with 2x sample buffer and were

resolved by SDS-PAGE electrophoresis and detected with anti-His (Cat No: 66005-1-Ig Proteintech, IL) or anti-GST (Cat No: G7781, Sigma, St. Louis, MO) antibodies.

Lynx1 antibody generation

An antibody against Lynx1 was developed following the methods previously outlined[71]. In brief, a piggyback transposon vector pXL-CAG-Zeomycin-2A and a piggyback transposase vector pCAG-mPBorf were obtained as a gift from Dr. Joshua Sanes. The Lynx1 sequence was cloned into the transposon vector following the 2A peptide sequence. L-cells were co-transfected with pXL-CAG-Zeomycin-2A-Lynx1 and pCAG-mPBorf. A stable cell line of Lynx1-expressing L-cells was generated by selection with Zeomycin and expression analysis confirmed the presence of Lynx1 mRNA. An antibody against mouse Lynx1 was generated by immunizing 1 month-old Lynx1-knockout mice with Lynx1-expressing L cells. Total serum was collected from immunized mice after six weeks of immunizations and purified using acetone powder. Antibody specificity was verified using transfected L cells and knockout mouse tissue.

Electrophysiology recordings:

Nerve-muscle preparations: Nerve–muscle preparations of the Extensor digitorum longus muscle (EDL) were dissected in oxygenated physiological solution (in mM): 110 NaCl, 5 KCl, 1 MgCl2, 25 NaHCO3, 2 CaCl2, 11 glucose, 0.3 glutamic acid, 0.4 glutamine, 5 BES (N,N-Bis(2-hydroxyethyl)-2-aminoethanesulfonic acid sodium salt), 0.036 choline chloride, and 4.34x10-7 cocarboxylase. After dissection, nerve muscle preparations were pinned in a Sylgard-coated recording chamber constantly perfused with oxygenated physiological solution (95%O2, 5%CO2). The pH (7.4) and temperature (28 ±2°C) were continuously regulated.

Recordings of synaptic transmission: Only recordings with an initial membrane potential larger than -65 mV and with less than 5 mV variation from holding potential were included in the analysis. NMJs were located using bright field illumination of an upright Olympus microscope with a 60X objective. Muscle fibers were impaled 50-100 µm from the NMJ to be studied, avoiding mechanical distortion of the NMJ.

Stimulation of the deep peroneal nerve was performed using a suction electrode filled with extracellular saline. Endplate potentials (EPPs) were recorded using glass microelectrodes (1.0 mm OD; WPI) pulled to 40-70 MΩ (filled with 3mM KCl) with a P-70 Brown-Flaming micropipette puller (Sutter Instruments). Synaptic responses were amplified by an AM Systems 1600 amplifier and further amplified (100x) and filtered (2 kHz) by a Warner Instruments DC amplifier. The recordings were digitized (10 KHz) using a National Instruments BNC 2110 board and subsequently acquired with WinWCP software (John Dempster, Strathclyde University, Strathclyde, UK).

Synaptic strength was determined by measuring the paired pulse facilitation (PPF) and the quantal content (m). These were obtained using a low Ca^{2+} (1mM) and high Mg^{2+} (7.0mM) modified physiological solution. Miniature endplate potentials (MEPPs) amplitude and frequency were first determined during a 5-10 min period of recordings without motor nerve stimulation. PPF was then obtained using two stimuli (0.1 ms duration, 10 ms interval), elicited at 0.2 Hz. Quantal content (m) was determined using the amplitude of the first EPP (EPP1) and MEPPs (mean EPP1s amp/mean MEPPs amp). Four to seven NMJs were studied per muscle.

Following a baseline recording of 20 min (0.2 Hz), synaptic plasticity was elicited by a sustained motor nerve stimulation (120 Hz, 10 s) followed by 45 min recordings of EPPs

558 evoked at 0.2 Hz. Muscle contractions were prevented with partial blockade of the
559 postsynaptic ACh receptors using D-tubocurarine (2.0 µM. Sigma). Only one NMJ was
560 studied per muscle.

561 *Muscular and neuromuscular strength and fatigue:* EDL nerve-muscle preparations were
562 attached to a fixed force transducer (model 402A-500mN, Aurora Scientific Inc) at one
563 end and an adjustable hook at the other end, using surgical thread. The knots for
564 attaching the muscle to the force transducer and the hook were done at the level of the
565 tendons, under a binocular, to prevent muscle fiber damage. Muscles were maintained
566 vertically in a 140 ml beaker containing oxygenated physiological solution. Two sets of
567 stimulating electrodes were then put in place. First, two platinum wires were positioned
568 on the muscle and on the tendon to stimulate the muscle directly. Second, the cut end of
569 the deep peroneal nerve was stabilized in a stimulating suction electrode filled with
570 extracellular saline. Nerve and muscle stimulations were performed either alternatively or
571 simultaneously.

572 Muscular and neuro-muscular twitch force responses were elicited by means of single
573 supra-maximal square-wave pulses lasting 1 ms and 0.1 ms, respectively. Optimal
574 muscle length was determined by incrementally stretching the muscle until maximum
575 neuro-muscular twitch force output was attained. After each length adjustment, a two-
576 minute rest period was allowed before the next stimulation.

577 The fatigue protocol consisted of bouts of motor nerve stimulations (120Hz, 300 ms) at
578 1Hz, for 3 min. Muscular stimulations were super-imposed on nerve stimulations at the
579 2^{nd}, 10^{th}, 20^{th}, 30^{th} stimulation, and so on until the end of the fatigue protocol so that both
580 muscular and neuromuscular fatigue could be measured. This was followed by a 30 min

recovery period where muscular and neuromuscular strength were measured at 2s, 5s, 10s, 15s, 30s, 1min, 1.5 min, 2 min, 2.5 m in, 5 min, 10 min, 20 min and 30 min following the fatigue protocol.

Immunohistochemistry and confocal microscopy of EDL muscles

EDL muscles from mice expressing YFP in nerve endings were used to visualize NMJs. Following perfusion, muscles were dissected and incubated with alexa-555 bungarotoxin (Life Technologies, 1:1000 in 1XPBS) for 1 hour. Muscles were then washed 3 times with 1XPBS and whole mounted using vectashield. NMJs were imaged using a Zeiss LSM 700 confocal microscope. Maximum intensity projections from confocal z-stacks were created using Zen Black (Zeiss) and analyzed using ImageJ.

NMJ Analysis: Structural features were analyzed based on previously described methods in Valdez et al. 2010[65]. In brief, full or partial denervation of NMJs is classified by inadequate apposition of YFP and BTX while fragmented nAChRs are defined as having 5 or more islands in the cluster. Sprouting NMJs are those with a nerve terminal overreaching the nAChR cluster. NMJs with multiple innervation are those with more than one axon innervating a single nAChR cluster. The endplate area is a measurement of the total area occupied by nAChR clusters in a single muscle. Colocalization is a measurement of YFP and BTX apposition analyzed using the ImageJ colocalization plugin. nAChR intensity was determined from the mean integrated density of nAChR clusters using ImageJ.

Immunohistochemistry and confocal microscopy of TA sections

Following perfusion, TA muscles were dissected and incubated in 30% sucrose for 48 hours at 4°C. Muscles were then cut in half and placed in Fisherbrand base molds with

Tissue Freezing Medium (Triangle Biomedical Sciences, Inc.) Using a cryostat, TA muscles were sectioned at 16 µm thickness and collected on gelatin-coated slides. Sections were first washed 3 times with 1XPBS and then incubated for 1 hour at room temperature with wheat germ agglutinin conjugated with alexa-555 (WGA, 1:700) and DAPI (4'6-diamidino-2-phenylindole: Sigma-Aldrich; 28718-90-3; 1:1,000) diluted in 1XPBS. Muscles were then washed 3 times with 1XPBS and whole mounted using vectashield. Muscle fibers were imaged using a Zeiss LSM 700 confocal microscope. Maximum intensity projections from confocal z-stacks were created using Zen Black (Zeiss) and analyzed using ImageJ. Muscle fibers were outlined by WGA and measured in ImageJ using the grid to randomly select at least 100 fibers per mouse to analyze fiber area. The percentage of centralized nuclei was then determined using the localization of DAPI in the outlined muscle fibers.

Immunohistochemistry and confocal microscopy for fiber-typing

TA muscles were immediately dissected following aesthesia with isoflurane and flash frozen in liquid nitrogen. Muscles were then cut in half and placed in Fisherbrand base molds with Tissue Freezing Medium (Triangle Biomedical Sciences, Inc.). Using a cryostat, TA muscles were sectioned at 16 µm thickness and collected on gelatin-coated slides. Sections were first washed 3 times with 1XPBS and then incubated for 1 hour at room temperature in blocking buffer (0.1% Triton X-100, 3% BSA, and 5% goat serum in 1XPBS). Next, sections were incubated with primary antibodies diluted in 3% BSA and 5% goat serum in 1XPBS overnight at 4°C. The following primary antibodies were used: rabbit-anti-laminin (1:300), IgG2b-BAD5 (1:20) to label MyHCI, IgM-BF-F3 (1:20) to label MyHCIIb, and IgG1-SC71 (1:40) to label MyHCIIa. Sections were then washed 3 times

with 1XPBS and incubated for 2 hours at room temperature with secondary antibodies and 4',6-diamidino-2-phenylindole (DAPI, Sigma, 1:1000). The following secondary antibodies were used: alexa-568 anti-mouse IgM (Life Technologies, 1:1000), alexa-488 donkey anti-rabbit (Life Technologies, 1:1000), and alexa-647 anti-mouse IgG1 (Life Technologies, 1:1000). Slides were then washed 3 times with 1XPBS and mounted using vectashield. Muscle sections were imaged using a Zeiss LSM 700 motorized confocal microscope. Maximum intensity projections from confocal z-stacks were created using Zen Black (Zeiss). The percentages of MyHCIIa and MyHCIIb fibers were determined based on the number of SC-71 and BF-F3 positive fibers, respectively.

qPCR expression analysis

Mice were anesthetized with isoflurane, and TA muscles were immediately dissected and flash frozen in liquid nitrogen. RNA was prepared using an Aurum Total RNA Mini kit (Bio-Rad), following the manufacturer's instructions. cDNA was then synthesized from 100ng of total RNA using an iScript cDNA synthesis kit (Bio-Rad). PCR amplification was performed on the Bio-Rad CFX Connect Real-Time System (Bio-Rad) using iTaq Universal SYBR Green Supermix (Bio-Rad). The primers used in this study are listed in Supplementary Table 1.

nAChR turnover analysis

The labeling of distinct nAChR pools was performed as described in Bruneau et al.,[47] with slight modification. Male C57/BL6 and Lynx1$^{-/-}$ mice, aged 148 days, were anesthetized by an intraperitoneal injection (5µL/g) of a mixed solution of ketamine (100mg/mL) and xylazine (20mg/mL) in sterile 0.9% saline. Each mouse was placed on its back and the sternomastoid muscle was surgically exposed. Muscles were bathed in saturating levels

of alexa 488-conjugated α-bungarotoxin (5μg/mL) for 1.5 h and then washed with sterile saline 3 times for 5 minutes. Two days following exposure, the animals were perfused transcardially with 4% PFA and the sternomastoid muscles were dissected. Muscles were then incubated with alexa 555-conjugated α-bungarotoxin (5μg/mL) for 1.5 h and then washed with sterile saline 3 times for 5 minutes each. Whole Sternomastoid muscles were mounted using vectashield and imaged with a Zeiss LSM 710 confocal microscope with the same scanning parameters. Maximum intensity projections from confocal z-stacks were created using Zen Black (Zeiss). The intensity of the 488 and 555 channels were analyzed at individual NMJs using ImageJ. The ratio of 555 to overall intensity was calculated for each NMJ and averaged for each animal. This ratio is considered the percentage of new nAChRs present.

Spinal Cord analysis

Spinal columns were dissected immediately after perfusion and post-fixed in 4% paraformaldehyde (PFA) overnight at 4°C. Following post-fixation, the spinal column was washed three times with 1xPBS and then cut in half at the last rib to separate the lumbar and sacral regions from the thoracic and cervical regions. The different regions of the spinal cord were isolated and placed in 30% sucrose overnight at 4°C. The spinal cord segments were then placed in a Fisherbrand base mold with Tissue Freezing Medium from Triangle Biomedical Sciences, Inc. Using a cryostat, 30 μm sections were collected on gelatin-coated slides and subsequently mounted using Vectashield. Ventral horns were imaged with a Zeiss LSM 900 confocal microscope with the same scanning parameters. Maximum intensity projections from confocal z-stacks were created using

Zen Black (Zeiss). The area of each motor neuron in the ventral horn was measured using ImageJ.

Statistics

For comparisons between two experimental groups, unpaired two-sided Student's t-tests were used to determine significance. For comparisons between two sample distributions, Kolmogorov–Smirnov tests were used to determine significance. Bar graphs are represented as means ± standard error. Data values and p-values are reported within the text. All measurements were taken from distinct samples with the sample size (*n*) listed in the figure legends. Statistical analysis was performed using R statistics software and GraphPad Prism7 with a p-value <0.05 was considered significant.

References

1. Sarter M, Bruno JP, Parikh V. Abnormal Neurotransmitter Release Underlying Behavioral and Cognitive Disorders: Toward Concepts of Dynamic and Function-Specific Dysregulation. *Neuropsychopharmacology*. 2007;32(7):1452-1461. doi:10.1038/sj.npp.1301285

2. Millar NS, Harkness PC. Assembly and trafficking of nicotinic acetylcholine receptors (Review). *Mol Membr Biol*. 2008;25(4):279-292. doi:10.1080/09687680802035675

3. Missias AC, Chu GC, Klocke BJ, Sanes JR, Merlie JP. Maturation of the acetylcholine receptor in skeletal muscle: regulation of the AChR gamma-to-epsilon switch. *Dev Biol*. 1996;179(1):223-238. doi:10.1006/dbio.1996.0253

4. Schaeffer L, De Kerchove D'Exaerde A, Changeux JP. Targeting transcription to the neuromuscular synapse. *Neuron*. 2001;31(1):15-22. doi:10.1016/S0896-6273(01)00353-1

5. Yumoto N, Wakatsuki S, Sehara-Fujisawa A. The acetylcholine receptor γ-to-ε switch occurs in individual endplates. *Biochem Biophys Res Commun*. 2005;331(4):1522-1527. doi:10.1016/j.bbrc.2005.04.081

6. Witzemann V, Schwarz H, Koenen M, et al. Acetylcholine receptor ε-subunit deletion causes muscle weakness and atrophy in juvenile and adult mice. *Proc Natl Acad Sci U S A*. 1996;93(23):13286-13291. doi:10.1073/pnas.93.23.13286

7. Middleton L, Ohno K, Christodoulou K, et al. Chromosome 17p-linked myasthenias stem from defects in the acetylcholine receptor epsilon-subunit gene. *Neurology*. 1999;53(5):1076-1082. doi:10.1212/wnl.53.5.1076

8. Ohno K, Anlar B, Özdirim E, Brengman JM, Engel AG. Frameshifting and splice-site mutations in the acetylcholine receptor ε subunit gene in three Turkish kinships with congenital myasthenic syndromes. In: *Annals of the New York Academy of Sciences*. Vol 841. Blackwell Publishing Inc.; 1998:189-194. doi:10.1111/j.1749-6632.1998.tb10926.x

9. Ohno K, Anlar B, Özdirim E, Brengman JM, DeBleecker JL, Engel AG. Myasthenic syndromes in Turkish kinships due to mutations in the acetylcholine receptor. *Ann Neurol*. 1998;44(2):234-241. doi:10.1002/ana.410440214

10. Ohno K, Quiram PA, Milone M, et al. Congenital myasthenic syndromes due to heteroallelic nonsense/missense mutations in the acetylcholine receptor ε subunit

gene: Identification and functional characterization of six new mutations. *Hum Mol Genet*. 1997;6(5):753-766. doi:10.1093/hmg/6.5.753

11. Engel AG, Ohno K, Bouzat C, Sine SM, Griggs RC. End-plate acetylcholine receptor deficiency due to nonsense mutations in the ε subunit. *Ann Neurol*. 1996;40(5):810-817. doi:10.1002/ana.410400521

12. Croxen R, Young C, Slater C, et al. End-plate gamma- and epsilon-subunit mRNA levels in AChR deficiency syndrome due to epsilon-subunit null mutations. *Brain*. 2001;124(Pt 7):1362-1372. doi:10.1093/brain/124.7.1362

13. Misgeld T, Kummer TT, Lichtman JW, Sanes JR. Agrin promotes synaptic differentiation by counteracting an inhibitory effect of neurotransmitter. *Proc Natl Acad Sci U S A*. 2005;102(31):11088-11093. doi:10.1073/pnas.0504806102

14. Misgeld T, Burgess RW, Lewis RM, Cunningham JM, Lichtman JW, Sanes JR. Roles of neurotransmitter in synapse formation: development of neuromuscular junctions lacking choline acetyltransferase. *Neuron*. 2002;36(4):635-648. http://www.ncbi.nlm.nih.gov/pubmed/12441053. Accessed February 12, 2016.

15. Lanuza MA, Besalduch N, González C, et al. Decreased phosphorylation of delta and epsilon subunits of the acetylcholine receptor coincides with delayed postsynaptic maturation in PKC theta deficient mouse. *Exp Neurol*. 2010;225(1):183-195. doi:10.1016/J.EXPNEUROL.2010.06.014

16. Leenders AGM, Sheng Z-H. Modulation of neurotransmitter release by the second messenger-activated protein kinases: implications for presynaptic plasticity. *Pharmacol Ther*. 2005;105(1):69-84. doi:10.1016/j.pharmthera.2004.10.012

738 17. Smith DO, Williams KD, Emmerling M. Changes in acetylcholine receptor
739 distribution and binding properties at the neuromuscular junction during aging. *Int*
740 *J Dev Neurosci*. 1990;8(6):629-642.

741 18. Friese MB, Blagden CS, Burden SJ. Synaptic differentiation is defective in mice
742 lacking acetylcholine receptor β-subunit tyrosine phosphorylation. *Development*.
743 2007;134(23):4167-4176. doi:10.1242/dev.010702

744 19. Sugita S, Fleming LL, Wood C, et al. VAChT overexpression increases
745 acetylcholine at the synaptic cleft and accelerates aging of neuromuscular
746 junctions. *Skelet Muscle*. 2016;6(1). doi:10.1186/s13395-016-0105-7

747 20. Magalhães-Gomes MPS, Motta-Santos D, Schetino LPL, et al. Fast and slow-
748 twitching muscles are differentially affected by reduced cholinergic transmission in
749 mice deficient for VAChT: A mouse model for congenital myasthenia. *Neurochem*
750 *Int*. 2018;120. doi:10.1016/j.neuint.2018.07.002

751 21. Vaughan SK, Sutherland NM, Valdez G. Attenuating Cholinergic Transmission
752 Increases the Number of Satellite Cells and Preserves Muscle Mass in Old Age.
753 *Front Aging Neurosci*. 2019;11:262. doi:10.3389/fnagi.2019.00262

754 22. Palma E, Reyes-Ruiz JM, Lopergolo D, et al. Acetylcholine receptors from human
755 muscle as pharmacological targets for ALS therapy. *Proc Natl Acad Sci U S A*.
756 2016;113(11):3060-3065. doi:10.1073/pnas.1600251113

757 23. Melroy-Greif WE, Stitzel JA, Ehringer MA. Nicotinic acetylcholine receptors:
758 upregulation, age-related effects and associations with drug use. *Genes Brain*
759 *Behav*. 2016;15(1):89-107. doi:10.1111/gbb.12251

24. Arbour D, Tremblay E, Martineau E, Julien J-P, Robitaille R. Early and Persistent Abnormal Decoding by Glial Cells at the Neuromuscular Junction in an ALS Model. *J Neurosci*. 2015;35(2):688-706. doi:10.1523/JNEUROSCI.1379-14.2015

25. Rocha MC, Pousinha PA, Correia AM, Sebastião AM, Ribeiro JA. Early changes of neuromuscular transmission in the SOD1(G93A) mice model of ALS start long before motor symptoms onset. *PLoS One*. 2013;8(9):e73846. doi:10.1371/journal.pone.0073846

26. Pousinha PA, Correia AM, Sebastião AM, Ribeiro JA. The giant miniature endplate potentials frequency is increased in aged rats. *Neurosci Lett*. 2015;584:224-229. doi:10.1016/j.neulet.2014.10.035

27. Sugita S, Fleming LL, Wood C, et al. VAChT overexpression increases acetylcholine at the synaptic cleft and accelerates aging of neuromuscular junctions. *Skelet Muscle*. 2016;6(1):31. doi:10.1186/s13395-016-0105-7

28. Miwa JM, Miwa JM, Ibanez-Tallon I, et al. lynx 1, an Endogenous Toxin-like Modulator of Nicotinic Acetylcholine Receptors in the mammalian CNS. *Neuron*. 1999;23:0.

29. Parker RL, O'Neill HC, Henley BM, et al. Deletion of lynx1 reduces the function of α6* nicotinic receptors. Akaaboune M, ed. *PLoS One*. 2017;12(12):e0188715. doi:10.1371/journal.pone.0188715

30. George AA, Bloy A, Miwa JM, Lindstrom JM, Lukas RJ, Whiteaker P. Isoform-specific mechanisms of α3β4*-nicotinic acetylcholine receptor modulation by the prototoxin lynx1. *FASEB J*. 2017;31(4):1398-1420. doi:10.1096/fj.201600733R

782 31. Ibanez-Tallon I, Miwa JM, Wang HL, et al. Novel modulation of neuronal nicotinic
783 acetylcholine receptors by association with endogenous prototoxin lyn1. *Neuron*.
784 2002;33(6):893-903.

785 32. Nichols WA, Henderson BJ, Yu C, et al. Lynx1 Shifts 4 2 Nicotinic Receptor
786 Subunit Stoichiometry by Affecting Assembly in the Endoplasmic Reticulum. *J Biol*
787 *Chem*. 2014;289(45):31423-31432. doi:10.1074/jbc.M114.573667

788 33. Sajo M, Ellis-Davies G, Morishita H. Lynx1 Limits Dendritic Spine Turnover in the
789 Adult Visual Cortex. *J Neurosci*. 2016;36(36):9472-9478.
790 doi:10.1523/JNEUROSCI.0580-16.2016

791 34. Morishita H, Miwa JM, Heintz N, Hensch TK. Lynx1, a cholinergic brake, limits
792 plasticity in adult visual cortex. *Science*. 2010;330(6008):1238-1240.
793 doi:10.1126/science.1195320

794 35. Takesian AE, Bogart LJ, Lichtman JW, Hensch TK. Inhibitory circuit gating of
795 auditory critical-period plasticity. *Nat Neurosci*. 2018;21(2):218-227.
796 doi:10.1038/s41593-017-0064-2

797 36. Kobayashi A, Parker RL, Wright AP, et al. lynx1 Supports Neuronal Health in the
798 Mouse Dorsal Striatum During Aging: an Ultrastructural Investigation. *J Mol*
799 *Neurosci*. 2014;53(3):525-536. doi:10.1007/s12031-014-0352-1

800 37. Miwa JM, Walz A. Enhancement in Motor Learning through Genetic Manipulation
801 of the Lynx1 Gene. *PLoS One*. 2012;7(11). doi:10.1371/

802 38. Sanz E, Yang L, Su T, Morris DR, McKnight GS, Amieux PS. Cell-type-specific

isolation of ribosome-associated mRNA from complex tissues. *Proc Natl Acad Sci U S A*. 2009;106(33):13939-13944. doi:10.1073/pnas.0907143106

39. Hippenmeyer S, Vrieseling E, Sigrist M, et al. A developmental switch in the response of DRG neurons to ETS transcription factor signaling. *PLoS Biol*. 2005;3(5):e159. doi:10.1371/journal.pbio.0030159

40. Miwa JM, Stevens TR, King SL, et al. The Prototoxin lynx1 Acts on Nicotinic Acetylcholine Receptors to Balance Neuronal Activity and Survival In Vivo. *Neuron*. 2006;51(5):587-600. doi:10.1016/j.neuron.2006.07.025

41. Lyukmanova EN, Shulepko MA, Buldakova SL, et al. Water-soluble LYNX1 Residues Important for Interaction with Muscle-type and/or Neuronal Nicotinic Receptors. *J Biol Chem*. 2013;288(22):15888-15899. doi:10.1074/jbc.M112.436576

42. Sanes JR, Lichtman JW. Development of the Vertebrate Neuromuscular Junction. *Annu Rev Neurosci*. 1999;22(1):389-442. doi:10.1146/annurev.neuro.22.1.389

43. Zammit PS, Relaix F, Nagata Y, et al. Pax7 and myogenic progression in skeletal muscle satellite cells. *J Cell Sci*. 2006;119(9):1824-1832. doi:10.1242/jcs.02908

44. Venuti JM, Morris JH, Vivian JL, Olson EN, Klein WH. Myogenin is required for late but not early aspects of myogenesis during mouse development. *J Cell Biol*. 1995;128(4):563-576. doi:10.1083/jcb.128.4.563

45. Burden SJ, Yumoto N, Zhang W. The role of MuSK in synapse formation and neuromuscular disease. *Cold Spring Harb Perspect Biol*. 2013;5(5).

824 doi:10.1101/cshperspect.a009167

825 46. Lee Y, Rudell J, Ferns M. Rapsyn interacts with the muscle acetylcholine receptor
826 via α-helical domains in the α, β, and ε subunit intracellular loops. *Neuroscience*.
827 2009;163(1):222-232. doi:10.1016/j.neuroscience.2009.05.057

828 47. Bruneau E, Sutter D, Hume RI, Akaaboune M. Identification of Nicotinic
829 Acetylcholine Receptor Recycling and Its Role in Maintaining Receptor Density at
830 the Neuromuscular Junction In Vivo. 2005. doi:10.1523/JNEUROSCI.3169-
831 05.2005

832 48. Evans WJ, Lexell J. Human Aging, Muscle Mass, and Fiber Type Composition.
833 *Journals Gerontol Ser A Biol Sci Med Sci*. 1995;50A(Special):11-16.
834 doi:10.1093/gerona/50A.Special_Issue.11

835 49. Frontera WR, Miljkovic N, Lim J-Y, Miljkovic I. Aging of Skeletal Muscle Fibers. *Ann
836 Rehabil Med Rev Artic Ann Rehabil Med*. 2015;39(2):155-162.
837 doi:10.5535/arm.2015.39.2.155

838 50. Frontera WR, Reid KF, Phillips EM, et al. Muscle fiber size and function in elderly
839 humans: a longitudinal study. *J Appl Physiol*. 2008;105(2):637-642.
840 doi:10.1152/japplphysiol.90332.2008

841 51. Meyer MA. Identification of 17 highly expressed genes within mouse lumbar spinal
842 cord anterior horn region from an in-situ hybridization atlas of 3430 genes:
843 implications for motor neuron disease. *Neurol Int*. 2014;6(2):5367.
844 doi:10.4081/ni.2014.5367

52. Nabel EM, Morishita H. Regulating Critical Period Plasticity: Insight from the Visual System to Fear Circuitry for Therapeutic Interventions. *Front Psychiatry*. 2013;4:146. doi:10.3389/fpsyt.2013.00146

53. Thomsen MS, Arvaniti M, Jensen MM, et al. Lynx1 and Aβ1-42 bind competitively to multiple nicotinic acetylcholine receptor subtypes. 2016. doi:10.1016/j.neurobiolaging.2016.06.009

54. Nissen NI, Anderson KR, Wang H, et al. Augmenting the antinociceptive effects of nicotinic acetylcholine receptor activity through lynx1 modulation. *PLoS One*. 2018;13(7). doi:10.1371/journal.pone.0199643

55. Hall ZW. Alpha neurotoxins and their relatives: foes and friends? *Neuron*. 1999;23(1):4-5.

56. Shulepko MA, Lyukmanova EN, Kasheverov IE, Dolgikh DA, Tsetlin VI, Kirpichnikov MP. Bacterial expression of the water-soluble domain of lynx1, an endogenous neuromodulator of human nicotinic receptors. *Russ J Bioorganic Chem*. 2011;37(5):543-549. doi:10.1134/S1068162011050165

57. Banker BQ, Kelly SS, Robbins N. Neuromuscular transmission and correlative morphology in young and old mice. *J Physiol*. 1983;339:355-377.

58. Kelly SS. The effect of age on neuromuscular transmission. *J Physiol*. 1978;274(1):51-62. doi:10.1113/jphysiol.1978.sp012133

59. Tremblay E, Martineau É, Robitaille R. Opposite Synaptic Alterations at the Neuromuscular Junction in an ALS Mouse Model: When Motor Units Matter. *J*

Neurosci. 2017;37(37):8901-8918. doi:10.1523/JNEUROSCI.3090-16.2017

60. Willadt S, Nash M, Slater C. Age-related changes in the structure and function of mammalian neuromuscular junctions. *Ann N Y Acad Sci*. 2018;1412(1):41-53. doi:10.1111/nyas.13521

61. Courtney J, Steinbach JH. Age changes in neuromuscular junction morphology and acetylcholine receptor distribution on rat skeletal muscle fibres. *J Physiol*. 1981;320:435-447. doi:10.1113/jphysiol.1981.sp013960

62. Cheng A, Morsch M, Murata Y, Ghazanfari N, Reddel SW, Phillips WD. Sequence of Age-Associated Changes to the Mouse Neuromuscular Junction and the Protective Effects of Voluntary Exercise. *PLoS One*. 2013. doi:10.1371/journal.pone.0067970

63. Li Y, Lee Y i., Thompson WJ. Changes in Aging Mouse Neuromuscular Junctions Are Explained by Degeneration and Regeneration of Muscle Fiber Segments at the Synapse. *J Neurosci*. 2011. doi:10.1523/jneurosci.3590-11.2011

64. Valdez G, Heyer MP, Feng G, Sanes JR. The role of muscle microRNAs in repairing the neuromuscular junction. *PLoS One*. 2014;9(3):e93140. doi:10.1371/journal.pone.0093140

65. Valdez G, Tapia JC, Kang H, et al. Attenuation of age-related changes in mouse neuromuscular synapses by caloric restriction and exercise. *Proc Natl Acad Sci U S A*. 2010;107(33):14863-14868. doi:1002220107 [pii]10.1073/pnas.1002220107

66. Dalkin W, Taetzsch T, Valdez G. The Fibular Nerve Injury Method: A Reliable Assay

887 to Identify and Test Factors That Repair Neuromuscular Junctions. *J Vis Exp*.
888 2016;(114). doi:10.3791/54186

889 67. Deschenes MR, Kressin KA, Garratt RN, Leathrum CM, Shaffrey EC. Effects of
890 exercise training on neuromuscular junction morphology and pre- to post-synaptic
891 coupling in young and aged rats. *Neuroscience*. 2016;316:167-177.
892 doi:10.1016/j.neuroscience.2015.12.004

893 68. Feng G, Mellor RH, Bernstein M, et al. Imaging Neuronal Subsets in Transgenic
894 Mice Expressing Multiple Spectral Variants of GFP. *Neuron*. 2000;28(1):41-51.
895 doi:10.1016/S0896-6273(00)00084-2

896 69. Gingras J, Gawor M, Bernadzki KM, et al. α-Dystrobrevin-1 recruits Grb2 and α-
897 catulin to organize neurotransmitter receptors at the neuromuscular junction. *J Cell*
898 *Sci*. 2016. doi:10.1242/jcs.181180

899 70. Herrmann D, Straubinger M, Hashemolhosseini S. Protein kinase CK2 interacts at
900 the neuromuscular synapse with Rapsyn, Rac1, 14-3-3γ, and Dok-7 proteins and
901 phosphorylates the latter two. *J Biol Chem*. 2015. doi:10.1074/jbc.M115.647610

902 71. Goodman KM, Yamagata M, Jin X, et al. Molecular basis of sidekick-mediated cell-
903 cell adhesion and specificity. *Elife*. 2016;5:e19058. doi:10.7554/eLife.19058

904 **Acknowledgements**

905 This work was funded through grants from the National Institute on Aging (R01AG055545
906 and R56AG051501) and the National Institute of Neurological Disorders and Stroke
907 (R21NS106313) awarded to GV. A portion of this work was also funded from a grant from
908 Polish National Science Center (UMO-2018/29/B/NZ3/02675) awarded to TJP, and by a

grant from Canadian Institute for Health Research (MOP-111070) and a discovery grant from the Natural Science and Engineering Research Council to RR. SBA was a Banting research scholar from Canadian Institute for Health Research.

Author Contributions

Study concept and design: SKV, GV. Acquisition of data: SKV and GV contributed to all aspects of the manuscript, SBA and RR contributed to electrophysiological studies, TJP and BPS contributed to co-immunoprecipitation experiments, TM contributed to data analysis. Drafting the manuscript: SKV, SBA, GV, RR. Statistical analysis: SKV, SB, TM, GV. Obtained funding: GV, RR, and TJP.

Conflicts of Interest

The authors have no conflict of interest to declare.

Data Availability

Data generated from the experiments outlined in this manuscript are available upon request from the corresponding author.

Figures

Figure 1.

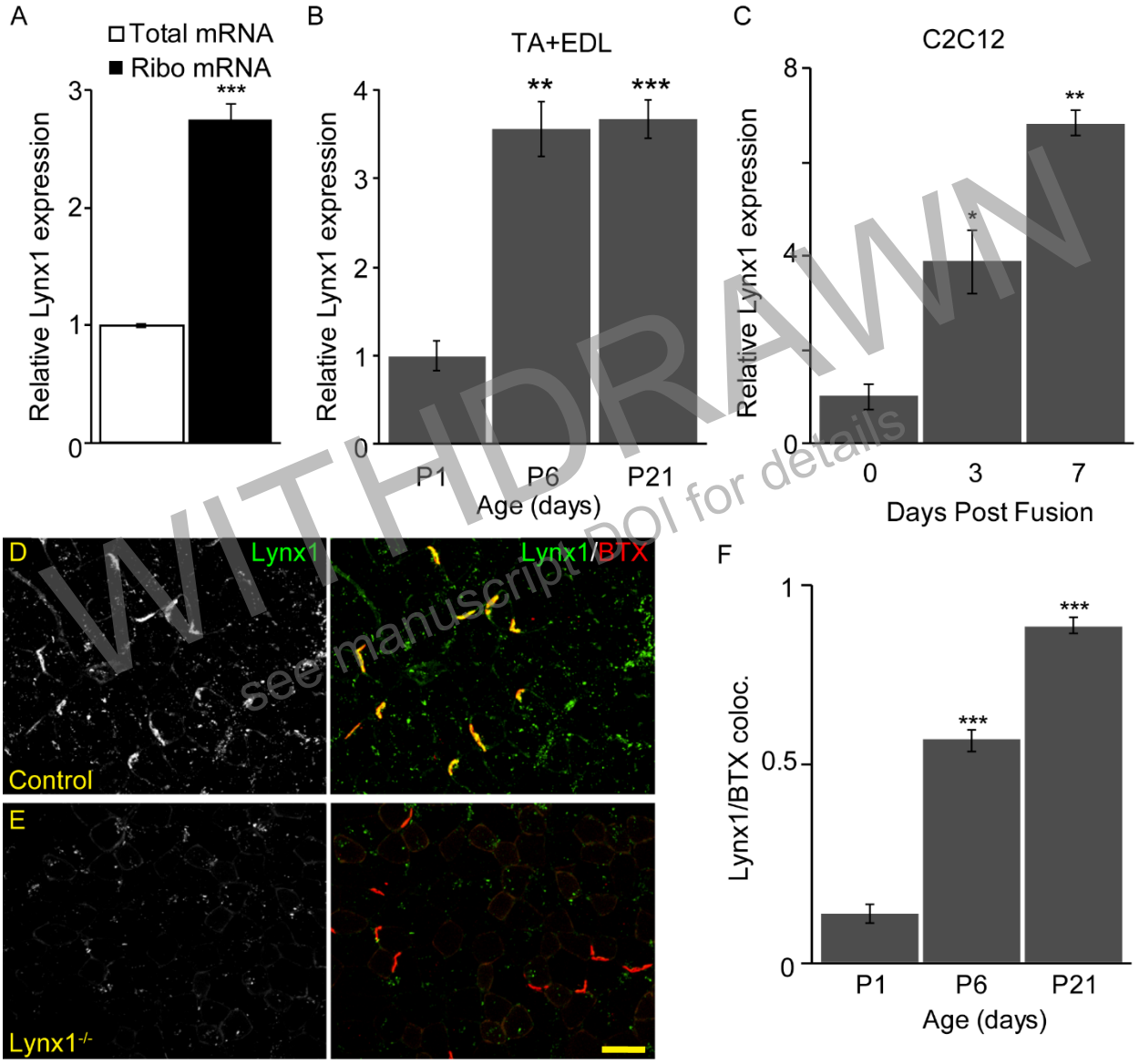

Figure 1. Skeletal muscles express Lynx1 at the NMJ. Lynx1 mRNA is enriched in ribosomal mRNA fractions obtained from adult TA muscle compared to total muscle mRNA (A). Lynx1 mRNA expression is detected in TA and EDL muscles and is significantly upregulated at postnatal day 6 (P6) and 21 (P21), relative to postnatal day 1 (P1) (B). Lynx1 mRNA is expressed in C2C12 myotubes and is significantly upregulated at 3 and 7 days post-fusion compared to unfused myoblasts (C). Lynx1 protein is colocalized with BTX in control TA muscles (D), but colocalization is not present in Lynx1$^{-/-}$ muscles (E). In control muscles, Lynx1 colocalization with BTX is significantly increased at P6 and P21, relative to P1 (F). Data represented as means ± SEM. Expression is normalized to GAPDH and relative to control. All male mice were used for this study. IP n=4; P1, P6, P21 n=5; C2C12 experiments were conducted with at least three biological replicates. D-E are representative images of P21 TA muscles. At least 30 NMJs were analyzed per animal (H). Scale bar=20 μm. Statistical significance was determined with unpaired and two-sided Student's t-tests. *p<0.05, **p<0.01, ***p<0.001.

Figure 2.

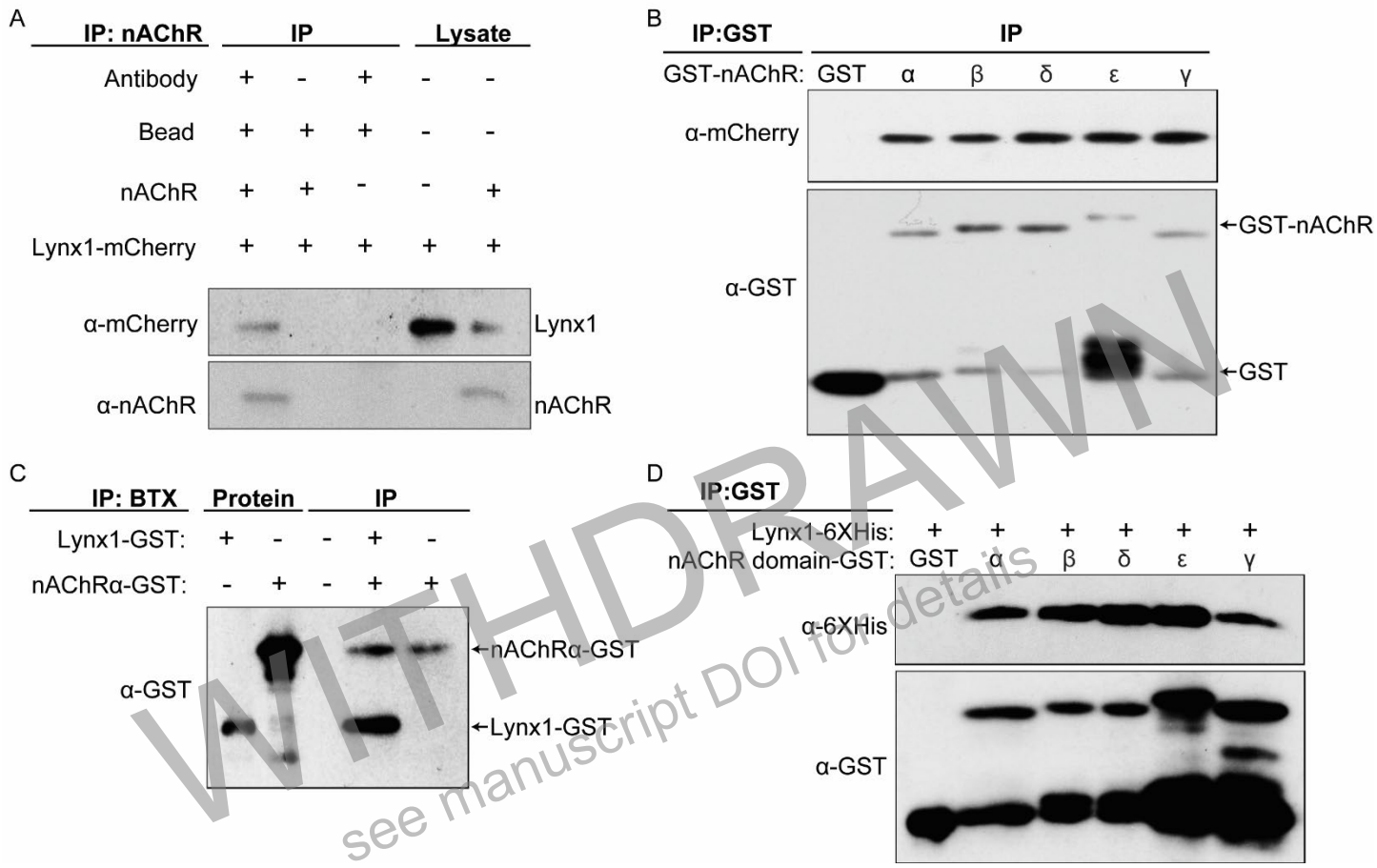

Figure 2. Lynx1 interacts with nAChRs. HEK293 cells were co-transfected with pLynx1-mCherry and four subunits of nAChR (α, β, δ and ε) that make functional receptors. The pull-down was performed with anti-nAChR antibody, and the blot was probed with anti-RFP or anti-nAChR antibodies. pLynx1-mCherry co-precipitates with nAChRs from HEK293 cell extract (A). The middle lane in the IP represents a control for precipitation specificity (beads without anti-nAChR antibody). The extracellular domains of each nAChR subunit (α, β, δ, ε and γ) were purified from bacteria and were analyzed for their ability pull-down Lynx1-Cherry from the HEK293 extract. The precipitates were analyzed by SDS-PAGE and Western blotting with anti-Cherry antibody. Lynx1 interacts with extracellular domains of muscle nAChR subunits (B). Arrows indicate the GST-nAChR fusion proteins and GST (control). Some truncation products containing GST were also detected. Based on the migration pattern, these additional bands likely represent the GST tag that was cleaved of the recombinant proteins. The GST-tagged extracellular domain of nAChRα subunit (nAChRα-GST) was analyzed for its ability to co-precipitate the purified GST-tagged Lynx1 (Lynx1-GST). The pull-down was performed with BTX-biotin attached to the Streptavidin Dynabeads, and the blot was probed with anti-GST antibody. Lynx1-GST co-precipitates with nAChRα-GST (C). The purified extracellular domains of each nAChR subunit (α, β, δ, ε and γ) were analyzed for their ability to pull-down the purified Lynx1-6XHis; GST was used as control (D). The precipitates were analyzed by SDS-PAGE and Western blotting with anti-His and anti-GST antibodies. Lynx1 interacts with extracellular domains of all muscle nAChR subunits. IP, immunoprecipitation.

Figure 3.

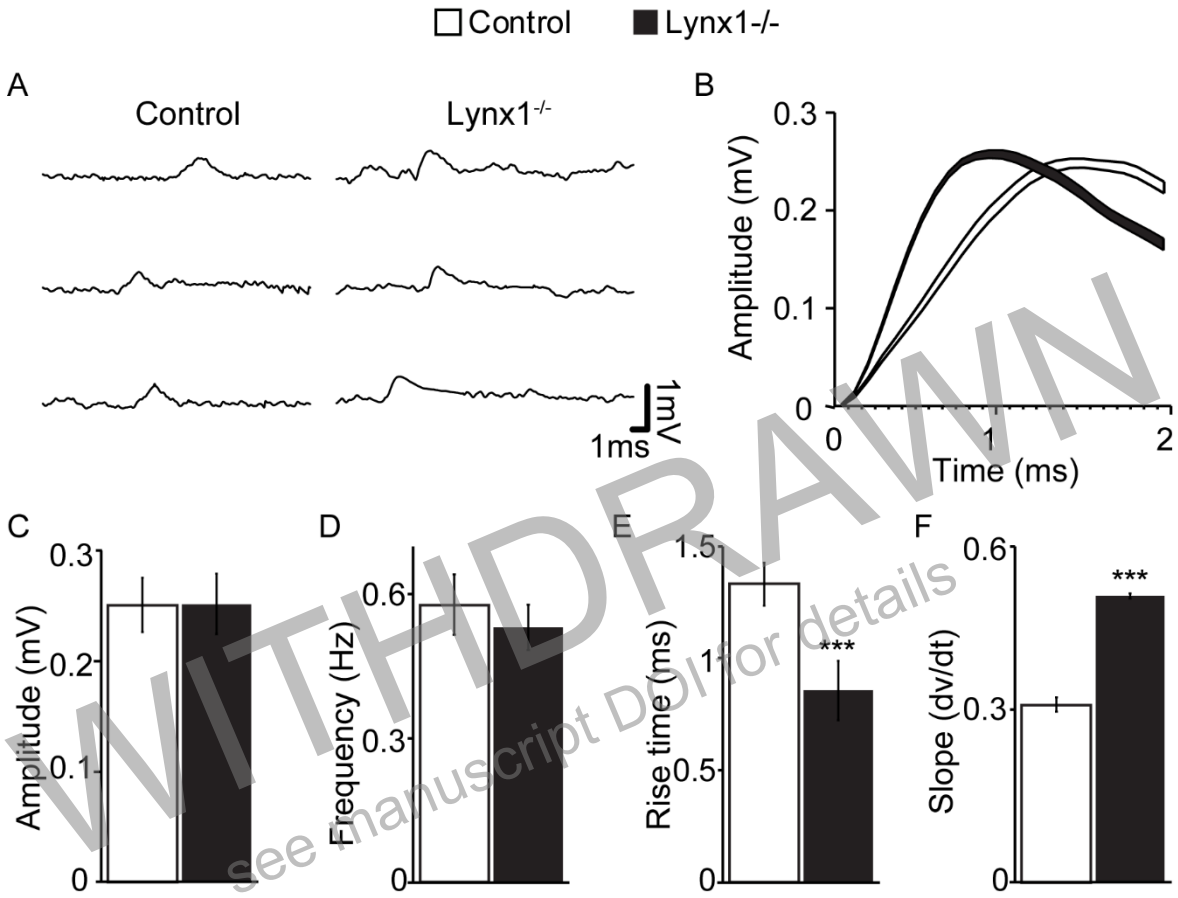

Figure 3. Increased sensitivity in nAChRs lacking Lynx1. Example traces of spontaneous MEPP recordings from control and Lynx1$^{-/-}$ mice (A). An average of 100 traces from control and Lynx1$^{-/-}$ MEPP recordings, where the line width represents SEM (B). The mean amplitude (C) and frequency (D) of MEPPs. The average MEPP rise time to peak amplitude (E) and the slope of MEPPs to peak amplitude (F) between control and Lynx1$^{-/-}$ mice. Data represented as means ± SEM. All male mice were used for this study. Control n=≥ 5, Lynx1$^{-/-}$ n=≥ 8. Statistical significance was determined with unpaired and two-sided Student's t-tests. ***p<0.001.

Figure 4.

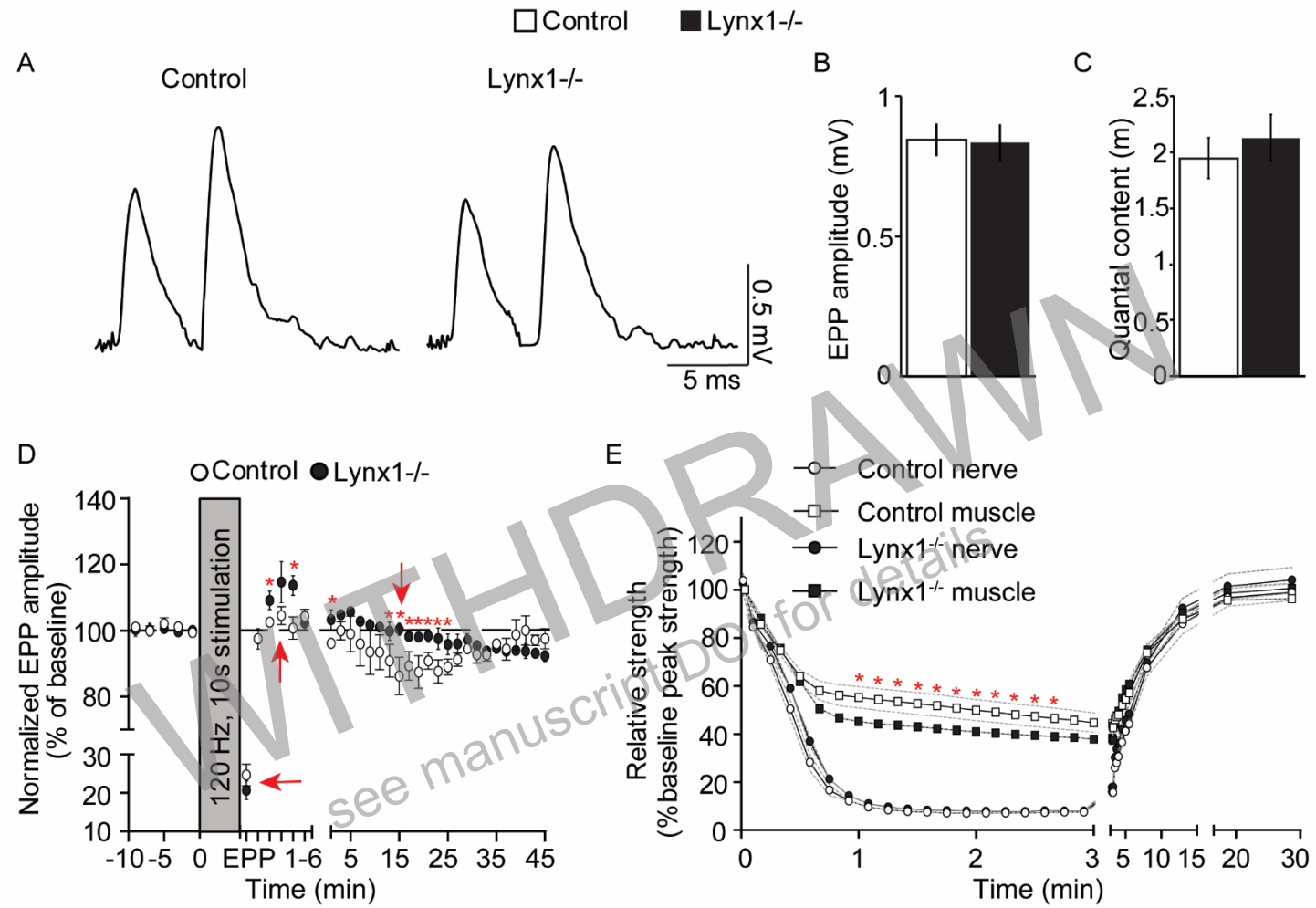

Figure 4. Lynx1 reduces synaptic plasticity and muscle force. Example of recordings of EPPs elicited by paired-pulse stimulation (0.2 Hz, 10 ms interval) from control and Lynx1$^{-/-}$ mice (A), the average EPP amplitude (measured of the first EPP of the pair) (B) and the average quantal content (C). Synaptic plasticity represented as amplitude of EPPs at baseline and following tetanic stimulation, arrows represent significant events (D). Neuromuscular fatigue represented as relative strength from baseline following super-imposed muscle and nerve stimulations after fatigue protocol (E). Data represented as means ± SEM. All male mice were used for this study. Control n=≥ 5, Lynx1$^{-/-}$ n=≥ 8. Statistical significance was determined with unpaired and two-sided Student's t-tests at each time point. *p<0.05.

Figure 5.

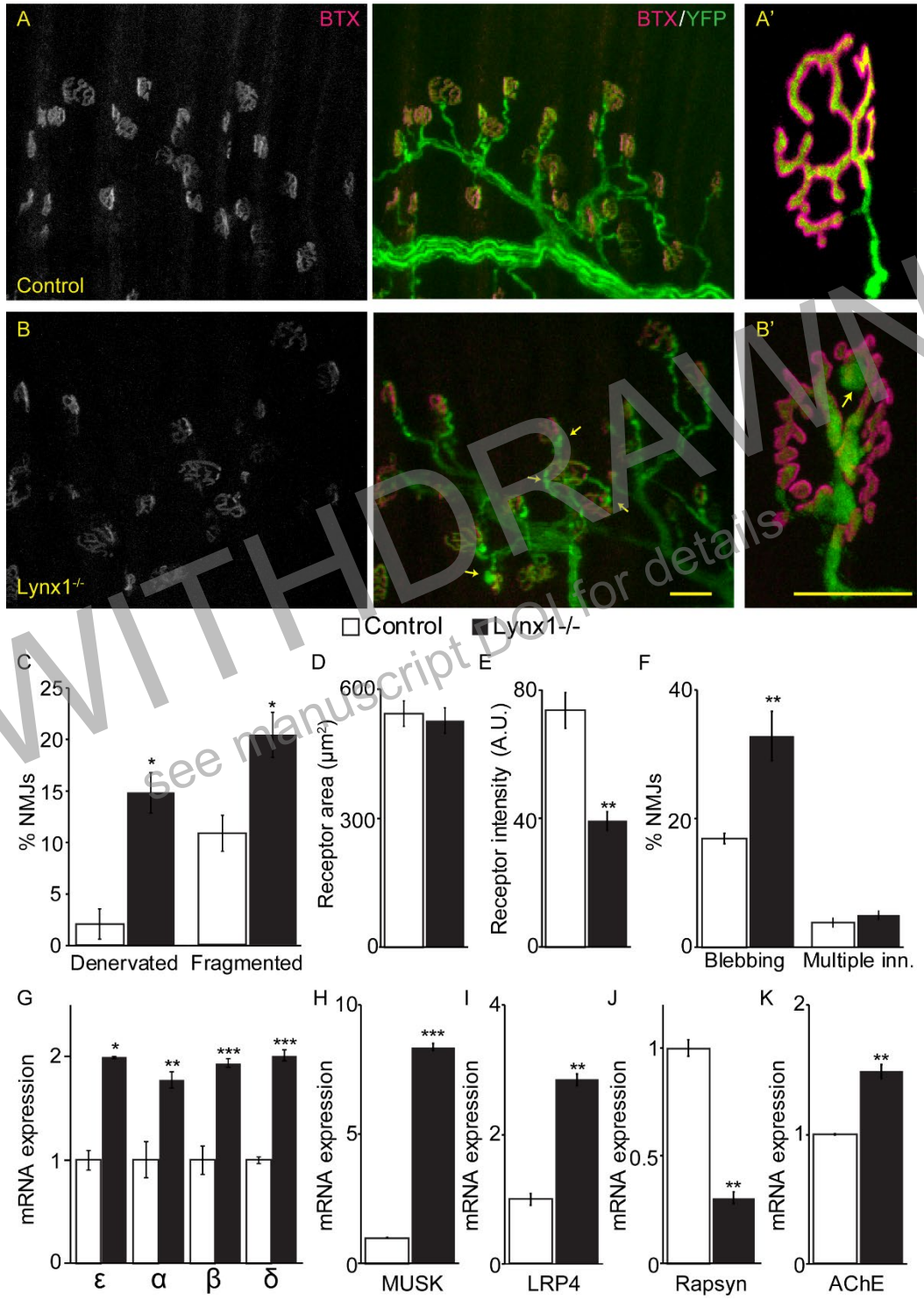

Figure 5. Lynx1 plays a role in NMJ maturation. Analysis of 4-month-old control (A) and Lynx1$^{-/-}$ (B) EDL muscles expressing YFP (green) in nerve endings and nAChRs visualized using BTX (red) shows increased NMJ denervation and fragmentation (B'; C) in Lynx1$^{-/-}$ muscles. The receptor area (D) is unaffected by Lynx1 deletion, but there is a significant decrease in receptor staining intensity (E) in Lynx1$^{-/-}$ mice. There are more blebs on innervating nerves (arrows), with no change in the incidence of multiple innervated nAChRs (F). However, qPCR analysis of 4-month-old TA muscle shows expression of all subunits in the mature muscle nAChR is significantly increased in Lynx1$^{-/-}$ muscles (G). Similarly, MuSK (H) and LRP4 (I) expression are significantly upregulated, while expression of Rapsyn (J) is significantly decreased in Lynx1$^{-/-}$ muscle. Expression of AChE is significantly increased in Lynx1$^{-/-}$ muscles (K). Data represented as means ± SEM. Expression is normalized to GAPDH and relative to control. All male mice were used for this study. Control n=4, Lynx1$^{-/-}$ n=5. At least 30 NMJs were analyzed per animal. Scale Bars=30μm. Statistical significance was determined with unpaired and two-sided Student's t-tests. *P<0.05, **P<0.01, ***P<0.001.

Figure 6.

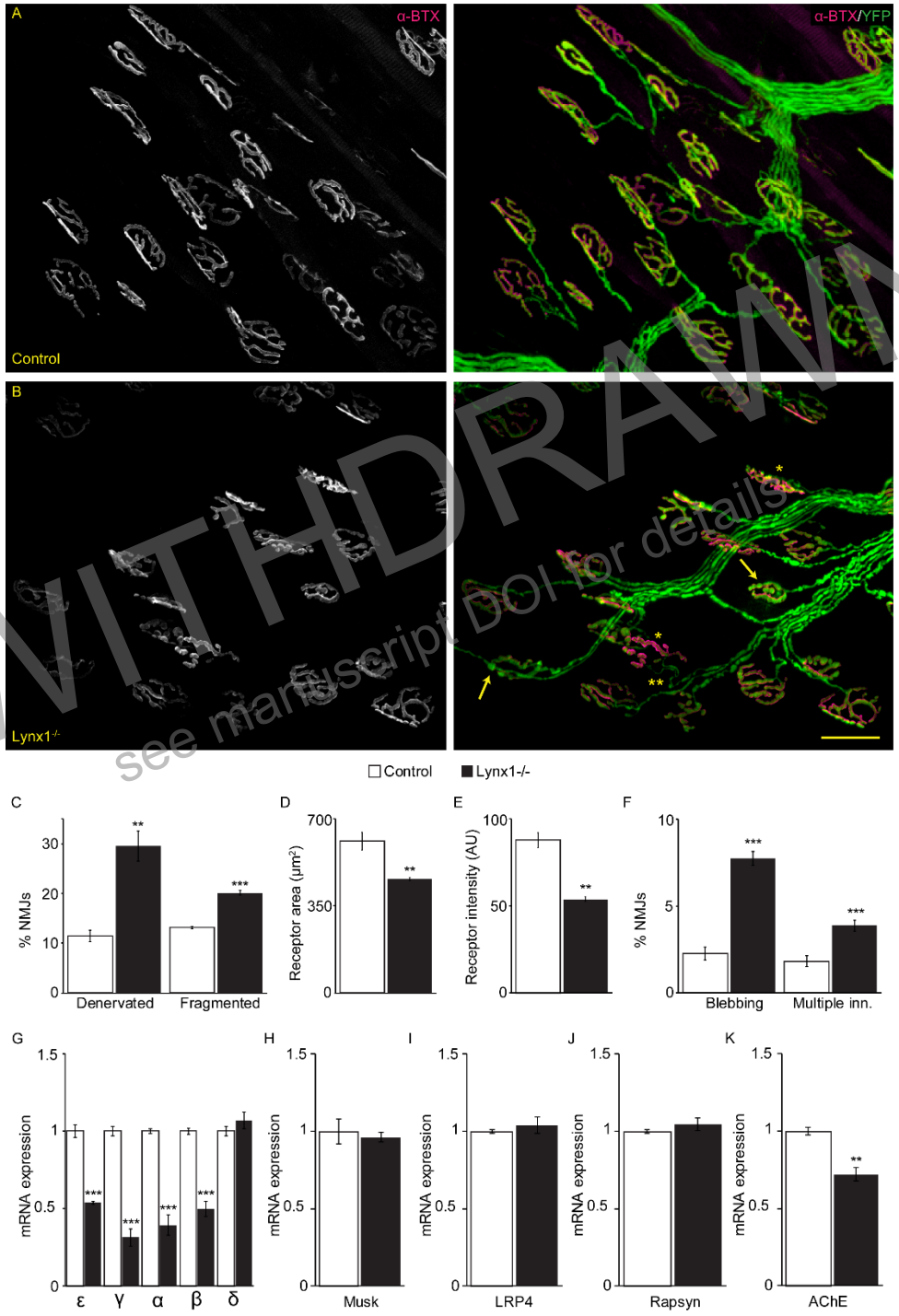

Figure 6. Lynx1 plays a role in NMJ maintenance. Analysis of 12-month-old control (A) and Lynx1$^{-/-}$ (B) EDL muscles expressing YFP (green) in nerve endings and nAChRs visualized using BTX (red) shows increased NMJ denervation and fragmentation in Lynx1$^{-/-}$ muscles (C; *). The area (D) and intensity (E) of nAChRs are also significantly reduced in Lynx1$^{-/-}$ muscles. Furthermore, there is an increase in the incidence of blebbing (arrows) on the innervating nerve and multiple innervated nAChRs (F; **). Expression of ε, γ, α, and β subunits is significantly reduced in Lynx1$^{-/-}$ TA muscles compared to controls (G). While the expression of MuSK (H), LRP4 (I), and Rapsyn (J) are unchanged. expression of AChE is reduced in Lynx1$^{-/-}$ TA muscles (K). Data represented as means ± SEM. Expression is normalized to GAPDH and relative to control. All male mice were used for this study. Control n=4, Lynx1$^{-/-}$ n=4. At least 30 NMJs were analyzed per animal. Scale Bar=30μm. Statistical significance was determined with unpaired and two-sided Student's t-tests. *P<0.05, **P<0.01, ***P<0.001.

Figure 7.

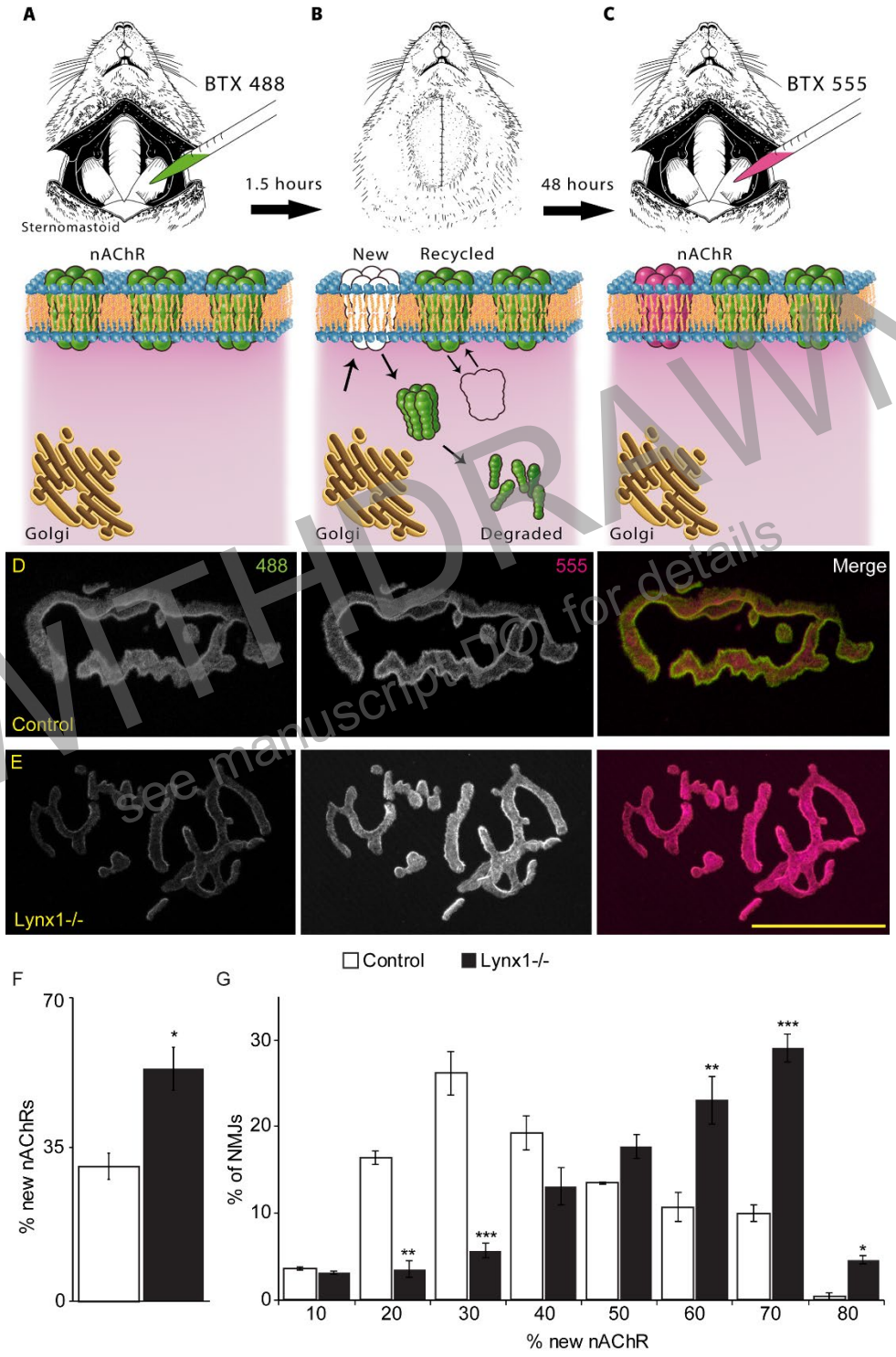

Figure 7. Loss of Lynx1 accelerates nAChR turnover in skeletal muscle. Sternomastoid muscles of 4-month-old mice were surgically exposed and bathed in saturating levels of BTX-488 (green) for 1.5 hours (A), then washed and sutured (B). After 48 hours, sternomastoid muscles were re-exposed and bathed in saturating levels of BTX-555 (red) for 1.5 hours (C). The ratio of intensity between BTX-488 and BTX-555 was determined in control (D) and Lynx1$^{-/-}$ (E) muscles. Lynx1$^{-/-}$ muscles have an increased percentage of newly labeled nAChRs (F). However, there is also substantial variability in nAChR turnover based on individual functional demands and morphological makeup of NMJs within the same muscles. The frequency distribution also shows an increase in the frequency of new nAChRs among NMJs in Lynx1$^{-/-}$ muscles (G). Data represented as means ± SEM. All male mice were used for this study. Control n=4, Lynx1$^{-/-}$ n=4. At least 50 NMJs were analyzed per animal. Scale Bar=30 µm. Statistical significance was determined with unpaired and two-sided Student's t-tests. *P<0.05, **P<0.01, ***P<0.001.

Figure 8.

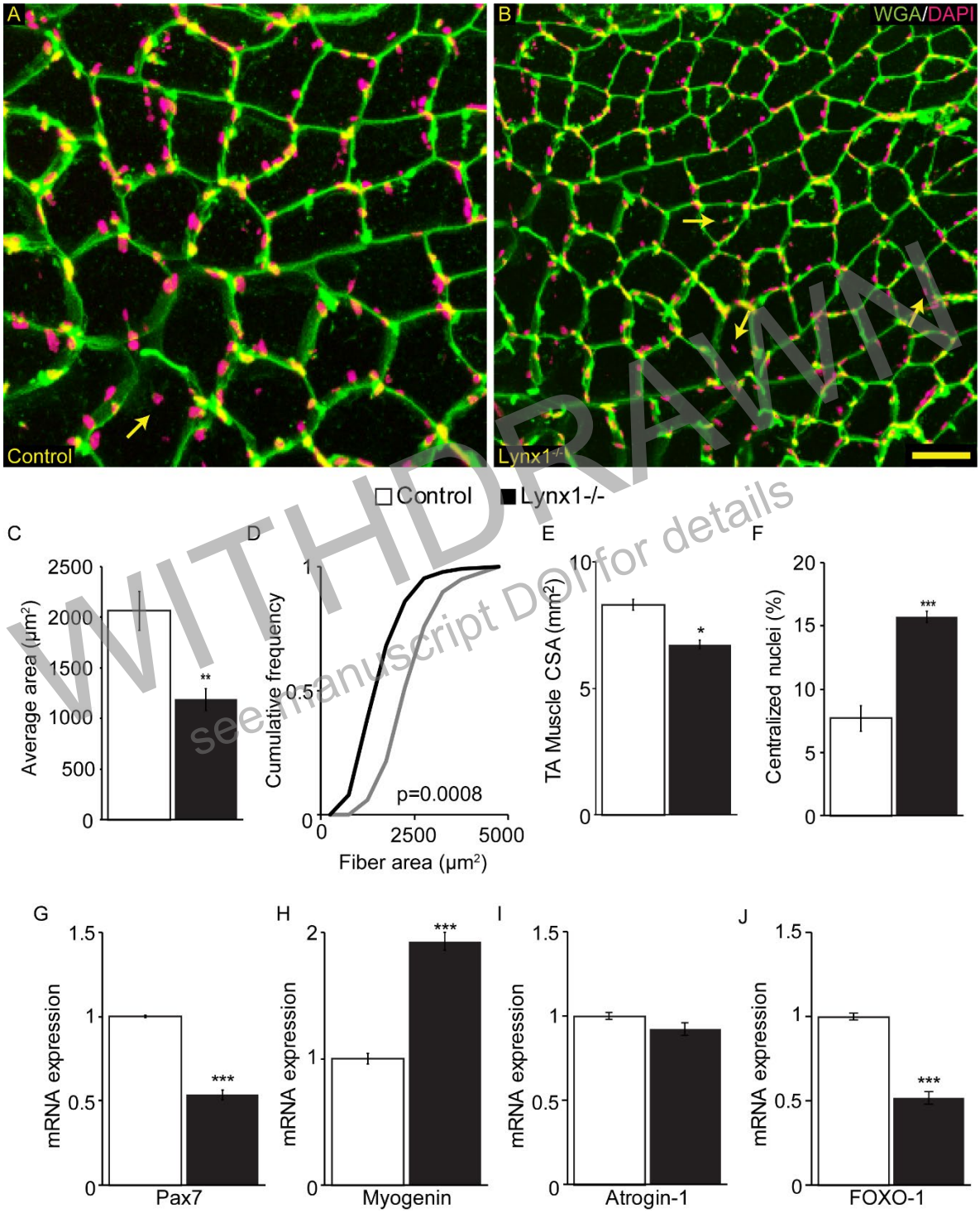

Figure 8. Muscle atrophy in aged Lynx1$^{-/-}$ mice. TA muscles from 12-month-old control (A) and Lynx1$^{-/-}$ (B) mice were cross-sectioned and stained with WGA (green) and DAPI (red) to visualize muscle fibers and their nuclei. Lynx1$^{-/-}$ muscles have a significantly decreased average cross-sectional area compared to controls (C). Similarly, the cumulative frequency distribution of cross-sectional area shows a significant reduction in Lynx1$^{-/-}$ muscles (D). The overall TA muscle CSA is also reduced in Lynx1$^{-/-}$ mice (E). Furthermore, Lynx1$^{-/-}$ muscles have an increase in the incidence of centralized nuclei compared to control muscles (F). Additionally, the mRNA expression of Pax7 is significantly reduced in Lynx1$^{-/-}$ muscles compared to controls (G). In contrast, myogenin expression is considerably increased (H), Atrogin-1 expression is unchanged (I), and FOXO-1 (J) expression is significantly reduced in Lynx1$^{-/-}$ muscles compared to controls. Data represented as means ± SEM. Expression is normalized to GAPDH and relative to control. All male mice were used for this study. Control n=4, Lynx1$^{-/-}$ n=4. At least 100 muscle fibers were analyzed per animal. Scale Bar=30μm. Statistical significance was determined with unpaired and two-sided Student's t-tests and Kolmogorov–Smirnov test (D). *P<0.05, **P<0.01, ***P<0.001.

Figure 9.

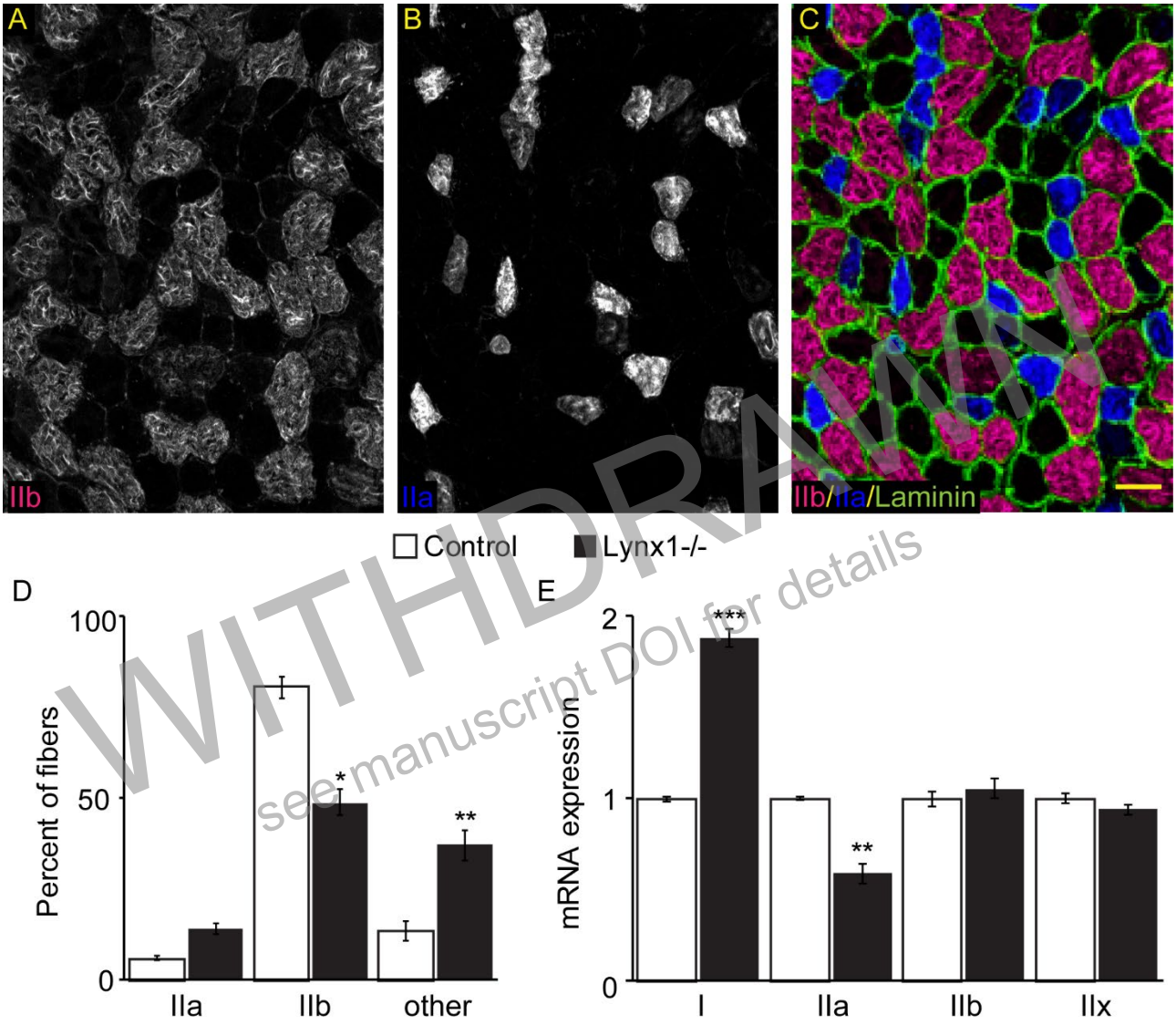

Figure 9. Fiber type shifts in aged Lynx1$^{-/-}$ muscles. TA muscles from 12-month-old control and Lynx1$^{-/-}$ mice were cross sectioned and stained with antibodies against MyHCIIb (A; red), MyHCIIa (B; blue), and laminin (C; green) to examine muscle fiber types. IHC analysis revealed a significant reduction in MyHCIIb fibers, and an increase in fibers that are either MyHCI or MyHCIIx in Lynx1$^{-/-}$ muscles (D). Further analysis of mRNA expression revealed a significant increase in MyHCI, and a reduction in MyHCIIa in Lynx1$^{-/-}$ muscles compared to controls (E). Data represented as means ± SEM. Expression is normalized to GAPDH and relative to control. All male mice were used for this study. Control n=4, Lynx1$^{-/-}$ n=4. At least 100 muscle fibers were analyzed per animal. Scale Bar=30μm. Statistical significance was determined with unpaired and two-sided Student's t-tests. *P<0.05, **P<0.01, ***P<0.001.

Figure 10.

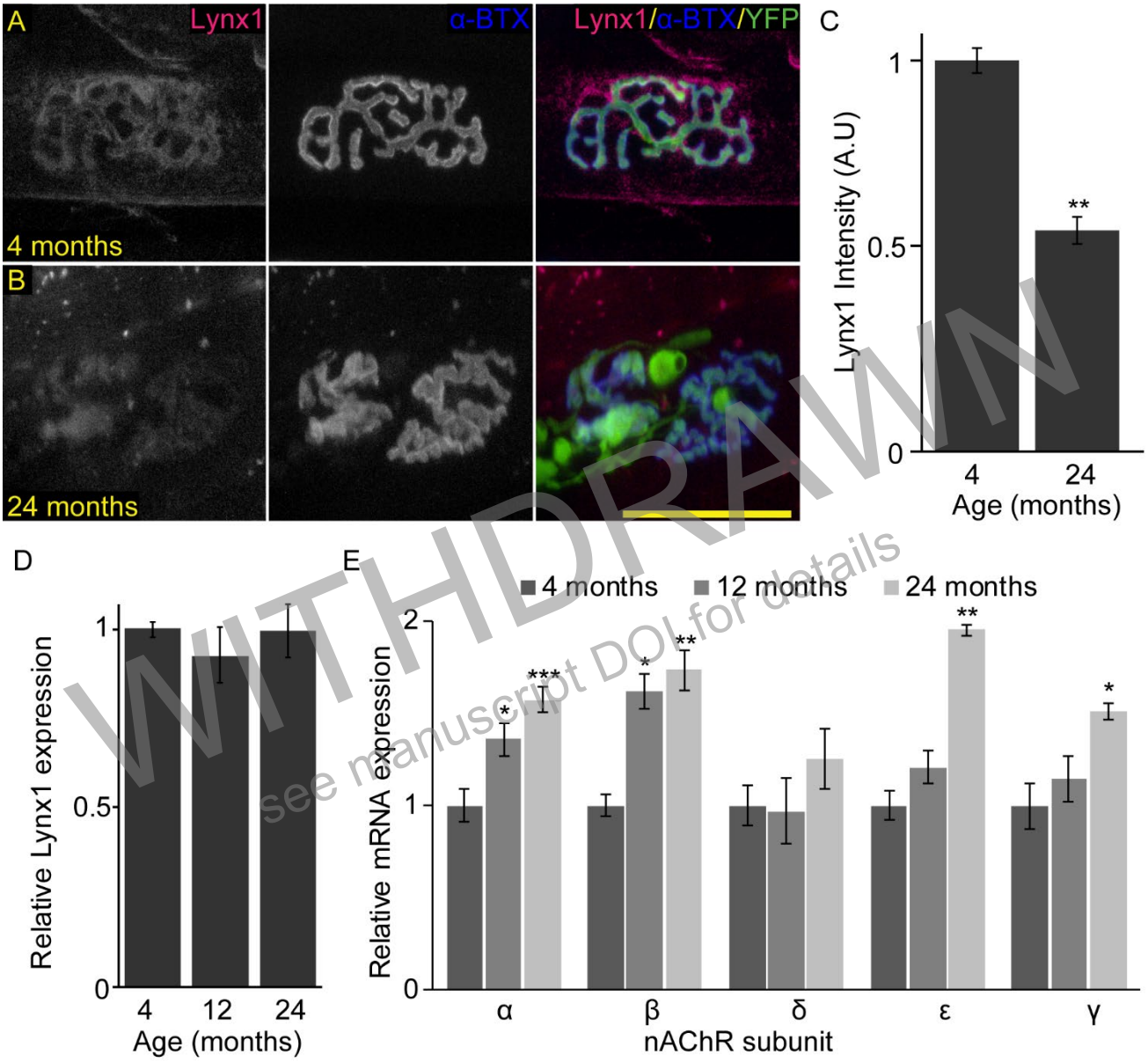

Figure 10. Endogenous Lynx1 expression in aging NMJs. Immunohistochemistry with anti-Lynx1 (red), BTX (blue), and YFP (green) revealed a loss of Lynx1 protein concentrated at the NMJ between 4 months (A) and 24 months of age (B, C). However, expression of Lynx1 remains constant in TA muscles from 4, 12, and 24 month-old animals (D). Expression of nAChR subunits (α, β, ε, and γ) is significantly increased in 24-month-old animals (E). Data represented as means ± SEM. Expression is normalized to GAPDH and relative to 4 months. All male mice were used for this study. 4 months; n=5, 12 months; n=5, 24 months; n=5. Scale Bar=30μm. Statistical significance was determined with unpaired and two-sided Student's t-tests. *P<0.05, **P<0.01, ***P<0.001.

Supplementary Figure 1.

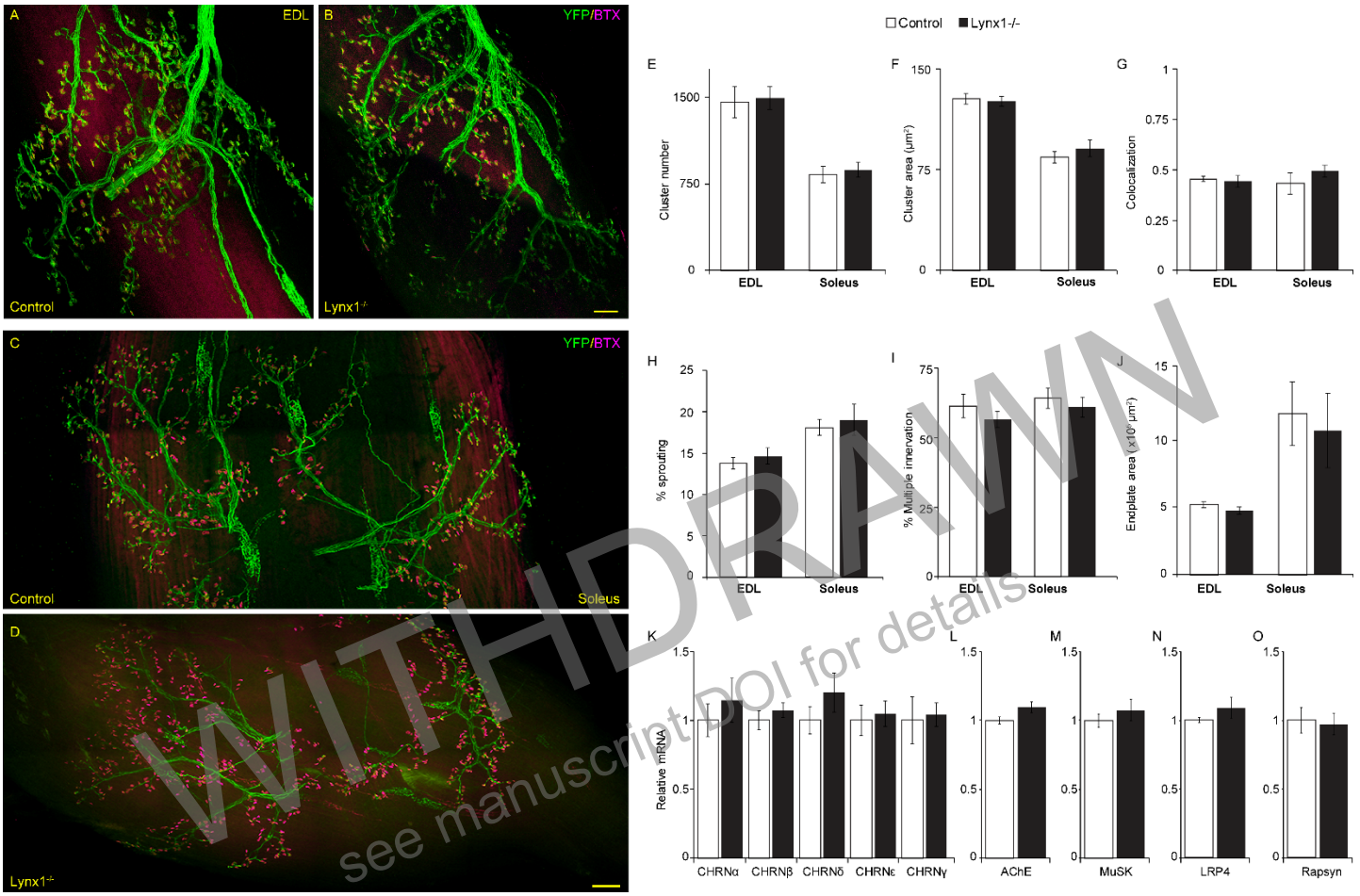

Supplementary Figure 1. Loss of Lynx1 has no discernable impact on NMJ development. The EDL (A,B) and soleus (C,D) muscles were examined from P6 control (A,C) and Lynx1$^{-/-}$ (B,D) mice expressing YFP (green) in nerve endings and nAChRs visualized using BTX (magenta). In both EDL and soleus muscles there are no differences in the number of nAChR plaques (E), the area of nAChR clusters (F), colocalization between YFP and BTX (G), sprouting of the nerve terminal (H), multiply innervated nAChR plaques (I), or the area of the endplate region (J) between control and Lynx1$^{-/-}$ muscles. Similarly, the mRNA expression of nAChR subunits (K), AChE (L), MuSK (M), LRP4 (N), or Rapsyn (O), are unchanged in Lynx1$^{-/-}$ TA muscles compared to controls. Data represented as mean ± SEM. Expression is normalized to GAPDH and relative to control. All male mice were used for this study. Control n = 5, Lynx1$^{-/-}$ n = 6. At least 50 NMJs were analyzed per animal. Scale bar = 20 μm.

Supplementary Figure 2.

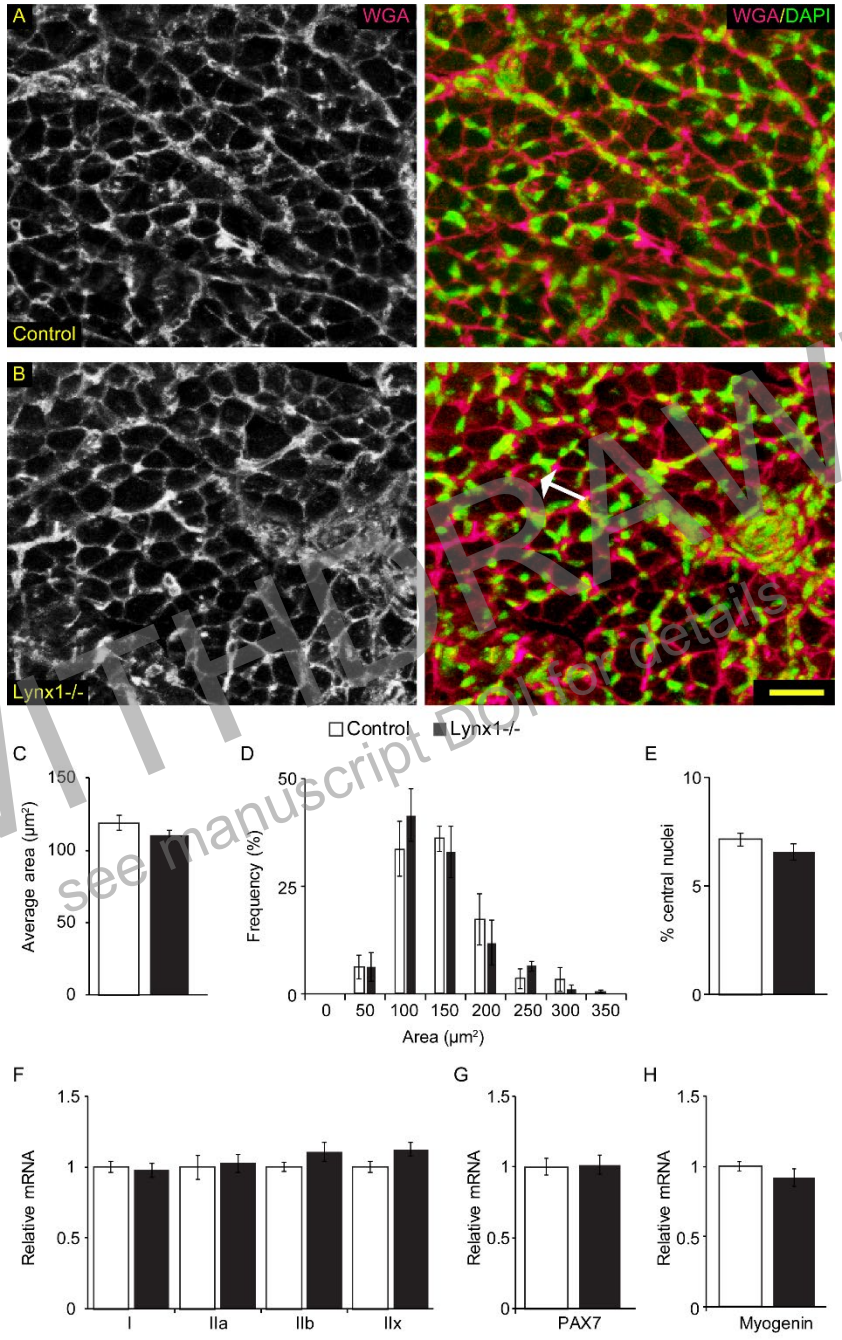

Supplementary Figure 2. Loss of Lynx1 has no effect on muscle fiber development. TA muscles from P6 control (A) and Lynx1$^{-/-}$ (B) mice were cross-sectioned and stained with WGA (magenta) and DAPI (green) to visualize muscle fibers and their nuclei. There is no difference in the average cross-sectional area of muscle fibers from control and Lynx1$^{-/-}$ muscles (C). Similarly, the frequency distribution of cross-sectional area is the same in control and Lynx1$^{-/-}$ muscles (D). There is also no difference in the incidence of centralized nuclei (white arrow) in control and Lynx1$^{-/-}$ muscles (E). Furthermore, the mRNA expression of myosin heavy chains is similar between Lynx1$^{-/-}$ muscles (F). The mRNA expression of Pax7 (G) and myogenin (H) is unchanged in Lynx1$^{-/-}$ TA muscles compared to controls. Data represented as mean ± SEM. Expression is normalized to GAPDH and relative to control. All male mice were used for this study. Control n = 5, Lynx1$^{-/-}$ n = 6. At least 100 muscle fibers were analyzed per animal. Scale bar = 20 μm.

Supplementary Figure 3.

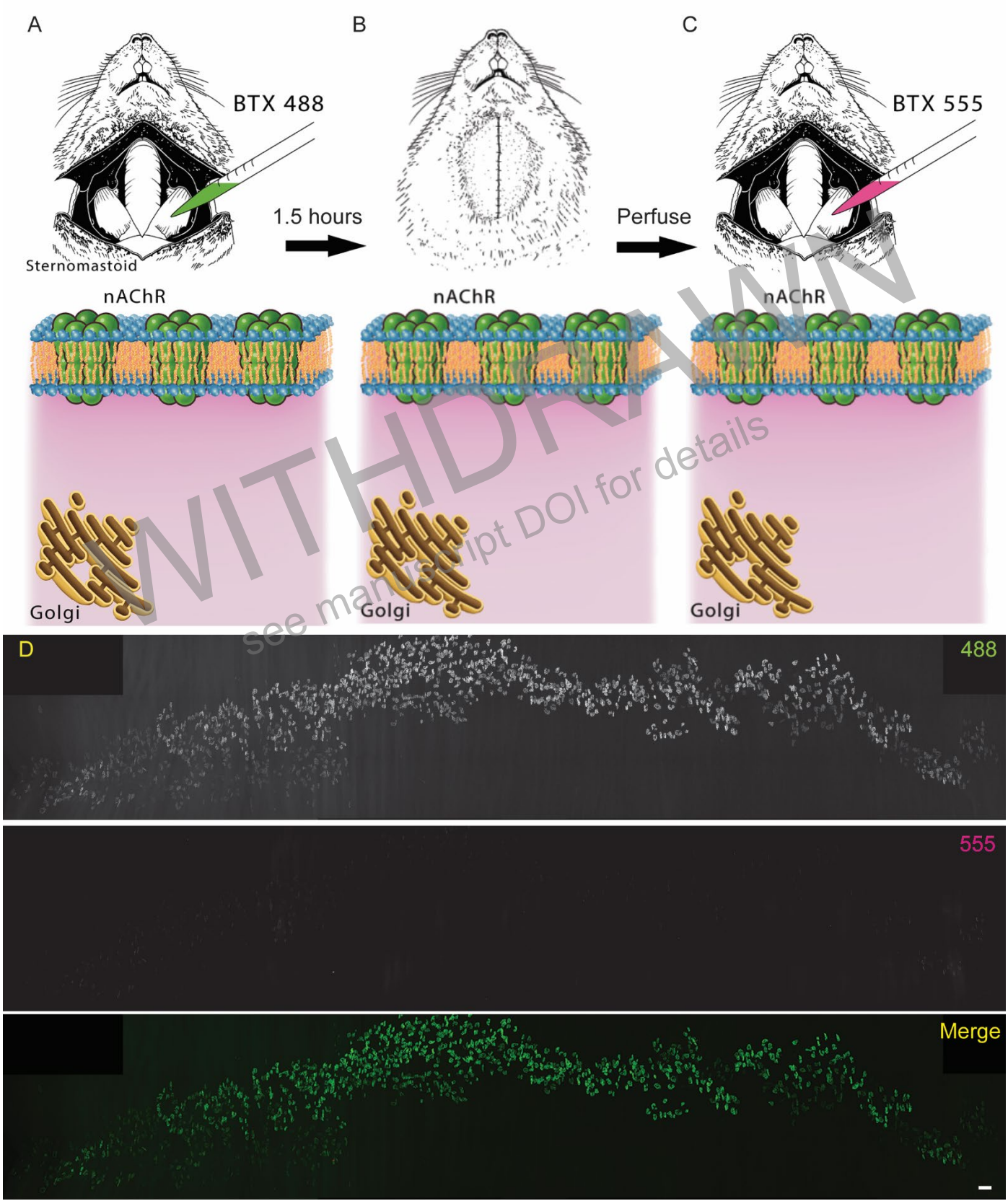

Supplementary Figure 3. nAChR saturation following BTX exposure. Sternomastoid muscles of 4 month-old mice were surgically exposed and bathed in saturating levels of BTX-488 (green) for 1.5 hours (A), then washed and immediately perfused (B). Sternomastoid muscles were subsequently bathed in saturating levels of BTX-555 (red) for 1.5 hours and then imaged (C). nAChRs are saturated by BTX-488, and are unlabeled by BTX-555 (D). Scale Bar=100μm.

Supplementary Figure 4.

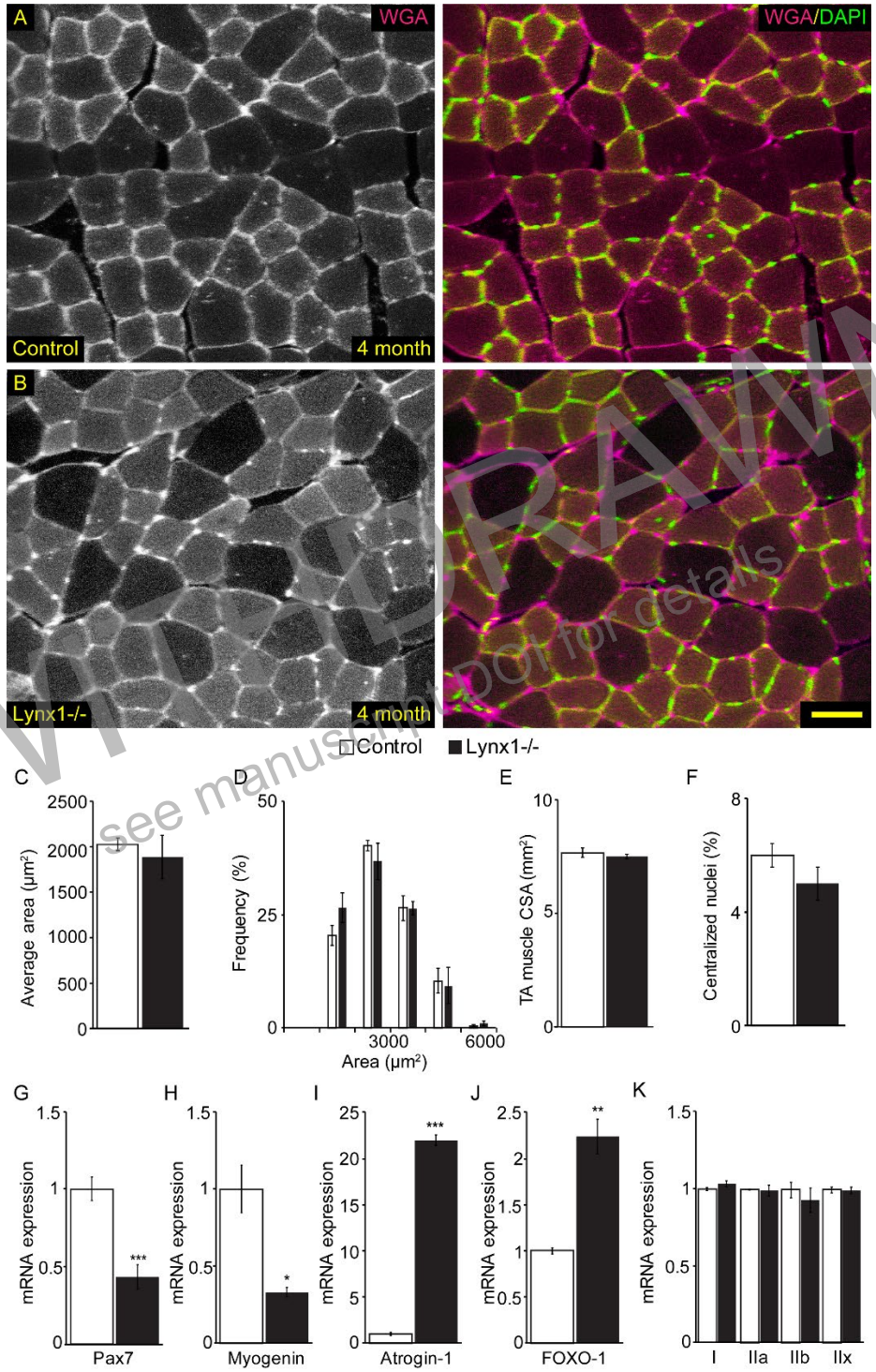

Supplementary Figure 4. Loss of Lynx1 increases signs of atrophy in adult muscle. TA muscles from 4 month-old control (A) and Lynx1$^{-/-}$ (B) mice were cross-sectioned and stained with WGA (magenta) and DAPI (green) to visualize muscle fibers and their nuclei. There is no difference in the average cross-sectional area of muscle fibers from control and Lynx1$^{-/-}$ muscles (C). Similarly, the frequency distribution of cross-sectional area is the same in control and Lynx1$^{-/-}$ muscles (D). Furthermore, there is no difference in the whole muscle CSA between control and Lynx1$^{-/-}$ TA muscles (E). There is also no difference in the incidence of centralized nuclei in control and Lynx1$^{-/-}$ muscles (F). However, the mRNA expression of Pax7 (G) and myogenin (H) is significantly reduced in Lynx1$^{-/-}$ muscles compared to controls. In contrast, Atrogin-1 (I) and FOXO-1 (J) expression is substantially increased in Lynx1$^{-/-}$ muscles compared to controls. However, the mRNA expression of myosin heavy chains is similar between Lynx1$^{-/-}$ muscles (K). Data represented as mean ± SEM. Expression is normalized to GAPDH and relative to control. All male mice were used for this study. Control n=4, Lynx1$^{-/-}$ n=4. At least 100 muscle fibers were analyzed per animal. Scale Bar=30µm. *P<0.05, **P<0.01, ***P<0.001.

Supplementary Figure 5.

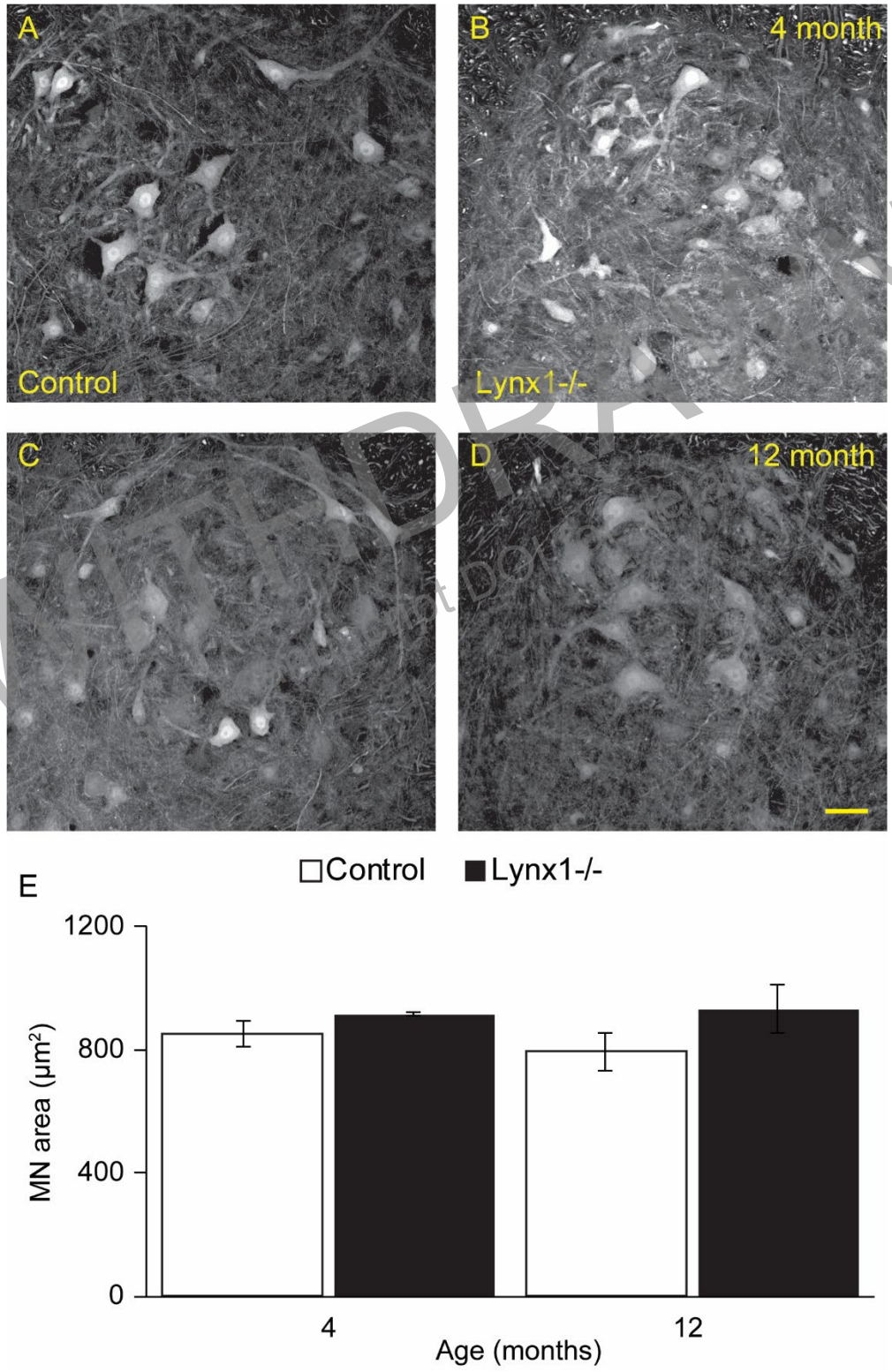

Supplementary Figure 5. No changes in motor neurons from Lynx1$^{-/-}$ mice.
Spinal cords from 4 month-old control (A) and Lynx1$^{-/-}$ (B) and 12 month-old control (C) and Lynx1$^{-/-}$ (D) mice were cross-sectioned. Motor neurons in the ventral horn were visualized using transgenic YFP expression. There is no difference in the average motor neuron area from control and Lynx1$^{-/-}$ spinal cords at 4 or 12 months of age (E). Data represented as mean ± SEM. All male mice were used for this study. Control n=4, Lynx1$^{-/-}$ n=4. At least 20 motor neurons were analyzed per animal. Scale Bar=50μm.

Table 1. qPCR primers

Gene	Fw (5'-3')	Rv (5'-3')
AChE	CTACACCACGGAGGAGAGGA	CTGGTTCTTCCAGTGCACCA
Atrogin-1	GCAGCAGCTGAATAGCATCCA	GGTGATCGTGAGGCCTTTGAA
CHRNα	CTTCAAAGAGCTTTGCCACC	CCATGGAGCTCTCGACTGTT
CHRNβ	AGGTCTCAGGCACTTTGTCG	TTCTACCTCCCACCAGATGC
CHRNδ	CCGATGCACTATCTCCCACT	CTTAGCCTGAAGCAGGAGGA
CHRNε	GCTGTGTGGATGCTGTGAAC	GCTGCCCAAAAACAGACATT
CHRNγ	GCTCAGCTGCAAGTTGATCTC	CCTCCTGCTCCATCTCTGTC
FOXO-1	GAGTTAGTGAGCAGGCTACATTT	TTGGACTGCTCCTCAGTTCC
GAPDH	CCCACTCTTCCACCTTCGATG	GTCCACCACCCTGTTGCTGTAG
LRP4	GGCAAAAAGCAGGAACTTGT	TCTACCCAGTGGCCAGAACT
Lynx1	ACCACTCGAACTTACTTCACC	ATCGTACACGGTCTCAAAGC
MUSK	CCGATGTGTCTGCTCTTTGA	ACAGGACAGTGGTGGAGGAC
Myogenin	ACCAGGAGCCCCACTTCTAT	GTCCCCAGTCCCTTTTCTTC
MyHCI	CTCAAGCTGCTCAGCAATCTATTT	GGAGCGCAAGTTTGTCATAAGT
MyHCIIa	GAGTGAGCAGAAGCGGAATGCT	GCGGAACTTGGATAGATTTGTG
MyHCIIb	CACCTGGACGATGCTCTCAGA	GCTCTTGCTCGGCCACTCT
MyHCIIx	GCTAGTAACATGGAGGTCA	TAAGGCACTCTTGGCCTTTATC
Pax7	GCGAGAAGAAAGCCAAACAC	GTCGGGTTCTGATTCCACAT
Rapsyn	GTGCCATGGAGTGTTGTGAG	CGGTTTCCGATCTCAGTCAT